

Leptogenesis in the presence of density perturbations

Kenta Hotokezaka^{1,*}, Ryusuke Jinno^{2,†}, Rin Takada^{1,‡}

¹ *Research Center for the Early Universe (RESCEU), Graduate School of Science,
The University of Tokyo, 7-3-1 Hongo, Bunkyo, Tokyo 113-0033, Japan*

² *Department of Physics, Graduate School of Science,
Kobe University, 1-1 Rokkodai, Kobe, Hyogo 657-8501, Japan*

(Dated: January 20, 2025)

We point out a new effect on the freeze-out process of heavy particles induced by density perturbations in the early universe, which we call “acoustically driven freeze-out.” This beyond-linear effect is caused by the exponential decoupling of heavy particles from the thermal bath in the presence of density perturbations, and already at moderately large values $\delta T/\bar{T} = \mathcal{O}(10^{-2})$ it cannot be captured by linear perturbation theory. We illustrate this effect with leptogenesis taking the decay and inverse decay of heavy neutrinos into account, and discuss its phenomenological implications. We found that perturbations always enhance the (spatially averaged) values of the final lepton asymmetry, and as a result, constraints on the mass of heavy neutrinos are found to be relaxed in the presence of perturbations.

I. INTRODUCTION

Inflation provides a successful explanation for the homogeneity, isotropy, and flatness of the universe [1–5] as well as the origin of the large-scale structure [6–9]. One of its characteristic predictions is that it generates density perturbations over different scales. While density perturbations are well constrained at large-scales from the Cosmic Microwave Background (CMB) [10] and large-scale structure observations [11], those at small scales are yet to be explored. These scalar fluctuations re-enter the Hubble horizon after inflation, driving acoustic oscillation of density and temperature.

Out-of-equilibrium phenomena play central roles in the history of the universe. One of the prominent examples is the production of baryon asymmetry, which requires out-of-equilibrium interactions among the Sakharov’s three conditions [12]. Other examples include preheating after inflation [13–15] and freeze-out/freeze-in of dark matter [16, 17], as well as Standard Model (SM) processes such as big bang nucleosynthesis (BBN) and recombination. Among these out-of-equilibrium processes, the effect we point out occurs when heavy particles decouple from the thermal bath. In the presence of temperature fluctuation δT , the Boltzmann factor for the equilibrium abundance of such particles with mass M is given by

$$\begin{aligned} \exp(-E/T) &= \exp[-E/(\bar{T} + \delta T)] \\ &= \exp(-E/\bar{T}) \exp(E\delta T/\bar{T}^2). \end{aligned} \quad (1)$$

When $E \simeq M$ is much larger than \bar{T} , the exponent of the second factor in the right-hand side of equation (1) is not necessarily smaller than unity, invalidating truncation of the system at the first order in perturbation. The

actual abundance of this particle species also closely follows this equilibrium value around the decoupling time, and hence the final abundance of this species itself or its decay product cannot also be predicted with truncation at the first order.

Baryogenesis is one of the phenomena in which this beyond-linear effect can potentially play an important role, and in this paper we illustrate the effect with one the simplest baryogenesis scenarios. *Leptogenesis* [18] is among the most successful scenarios, in which the Sakharov’s three conditions are satisfied by the CP-violating decay of right-handed neutrinos together with the sphaleron process in the SM. These right-handed neutrinos naturally exist in the UV completion of the SM such as grand unification theories, and can also naturally explain the masses of light neutrinos through the seesaw mechanism [19–22]. The masses, mixing angles, and CP phase(s) of these light neutrinos are being explored with solar, reactor, atmospheric and accelerator neutrino oscillation experiments (see e.g., Ref. [23]), while their Dirac or Majorana nature may be determined in the current or future $0\nu\beta\beta$ decay experiments (see e.g., Ref. [24]).

Density perturbations at small scales, on the other hand, are gaining interest in view of gravitational-wave (GW) observations [25–30]. They give rise to multipole structures in the matter distribution, and for sufficiently large amplitude they produce secondary GWs [31, 32] and lead to the formation of primordial black holes [33–35]. Part of the motivations of the current paper is reassessing the effect of inhomogeneous universe on particle physics processes, demonstrating the interplay of micro- and macro-physics. In this perspective, we investigate the influence of density perturbations on the lepton and baryon asymmetries within the simplest leptogenesis scenarios. As we see in the following, sound waves induce a sudden freeze-out of heavy particles, resulting in a net enhancement in the particle abundance after freeze-out

* kentah@resceu.s.u-tokyo.ac.jp

† jinno@phys.sci.kobe-u.ac.jp

‡ takada-rin@resceu.s.u-tokyo.ac.jp

even after spatial average.¹ We call this process “acoustically driven freeze-out.”

This paper is organized as follows. In Section II, we derive the Boltzmann equations for the heavy neutrino N_1 and for the baryon-minus-lepton number $B-L$, in the presence of density perturbations. We also review various parameters related to the neutrino masses. In Section III, we discuss the intuitive picture for the acoustically driven freeze-out, and then present the time evolution of the right-handed neutrino and $B-L$ as well as the parameter space for successful baryogenesis. Finally in Section IV we discuss the implications of our results and present possible future directions.

II. LEPTOGENESIS IN THE PRESENCE OF COSMOLOGICAL PERTURBATIONS

A. Prerequisites for leptogenesis

Leptogenesis [18] is a scenario in which the CP-violating decays of heavy right-handed neutrinos, together with the sphaleron process in the SM, generate the baryon asymmetry of the universe. In leptogenesis, the SM is extended with right-handed neutrinos with heavy Majorana masses that violate the lepton number. These right-handed neutrinos have Yukawa interactions with the Higgs and light leptons, whose complex phases give rise to CP violation. Their CP-violating decays produce lepton asymmetry, part of which is then converted into baryon asymmetry through the SM sphaleron process. The Majorana masses of the right-handed neutrinos at the same time explain the observed light masses for left-handed neutrinos via the seesaw mechanism.

Leptogenesis scenarios can be classified into two classes: thermal and non-thermal (see, e.g., [37, 38]). The former assumes thermal abundance for the right-handed neutrinos as one of the initial conditions, while in the latter the right-handed neutrinos are produced via various non-thermal processes. One of the attractive features of the former class is its robust predictivity: the number of free parameters is significantly smaller, thereby allowing for more robust experimental predictions. For this reason we focus on thermal leptogenesis in this paper.

We consider a simple model so-called vanilla leptogenesis, in which heavy right-handed neutrinos N_1 , N_2 , and N_3 with masses in the order $M_1 < M_2 < M_3$ are added

to the SM. In this model, the Majorana mass terms and Yukawa couplings of the right-handed neutrinos

$$\mathcal{L} = -\frac{M_\alpha}{2} \bar{N}_\alpha N_\alpha - y_{\alpha\beta} \phi^* \bar{l}_\alpha N_\beta + \text{h.c.}, \quad (2)$$

are added to the SM Lagrangian together with their kinetic terms. Here M_α and $y_{\alpha\beta}$ denote the Majorana masses and Yukawa couplings, respectively, while ϕ and l_α are the Higgs and lepton doublets of the SM, respectively. The summation over lepton flavors $\alpha, \beta = 1, 2, 3$ is implicit. The light neutrino masses are generated from the type-I seesaw mechanism [19–22].

The lightest right-handed neutrino N_1 decays into a lepton doublet and Higgs doublet pair or its CP-conjugate:

$$N_1 \rightarrow l_\alpha \phi, \quad N_1 \rightarrow \bar{l}_\alpha \phi^*. \quad (3)$$

In this paper, only the decay and inverse decay of N_1 are included, and scattering processes are ignored. The decays of N_2 and N_3 are assumed to be negligible in the final asymmetry, and they appear only as internal lines in the diagrams of N_1 decay. This simplified model is sufficient to capture the beyond-linear effect we point out in the present study. The $B-L$ asymmetry is generated from the CP-violating decays (3) as

$$\frac{\Gamma(N_1 \rightarrow l_\alpha \phi)}{\Gamma(N_1 \rightarrow l_\alpha \phi) + \Gamma(N_1 \rightarrow \bar{l}_\alpha \phi^*)} = \frac{1 + \varepsilon_1}{2}, \quad (4)$$

$$\frac{\Gamma(N_1 \rightarrow \bar{l}_\alpha \phi^*)}{\Gamma(N_1 \rightarrow l_\alpha \phi) + \Gamma(N_1 \rightarrow \bar{l}_\alpha \phi^*)} = \frac{1 - \varepsilon_1}{2}.$$

Here the parameter $\varepsilon_1 (< 0)$ describing CP asymmetry is given by (see Appendix D)

$$\varepsilon_1 = \sum_{\gamma=2,3} \frac{\text{Im}(y_{\alpha 1} y_{\beta 1} y_{\alpha \gamma}^* y_{\beta \gamma}^*)}{8\pi \sum_\alpha |y_{\alpha 1}|^2} f(x), \quad x \equiv \frac{M_\gamma^2}{M_1^2} \quad (5)$$

$$f(x) \equiv \sqrt{x} \left[1 + \frac{1}{1-x} - (1+x) \ln \left(1 + \frac{1}{x} \right) \right].$$

In the following, we consider the time evolution of the ratios $N_{N_1} \equiv n_{N_1}/n_\gamma$ and $N_{B-L} \equiv (n_B - n_L)/n_\gamma$, where n_{N_1} , n_γ , n_B , and n_L denote the number densities of right-handed neutrinos, photons, baryons, and leptons, respectively. Their initial conditions are given at sufficiently high temperatures $T \gg M_1$ by

$$N_{N_1}^{\text{eq}}(T \gg M_1) = \frac{n_{N_1}^{\text{eq}}}{n_\gamma^{\text{eq}}} = \frac{3}{4}, \quad N_{B-L}^{\text{eq}}(T \gg M_1) = 0. \quad (6)$$

After the decay of right-handed neutrinos, the negative lepton number L is converted into positive B and negative L through the sphaleron process [39, 40]. Since $B-L$ is conserved in this process, the final baryon number B is related to the value of $B-L$ generated by N_1 decay as [41, 42]

$$B = \frac{8\nu_f + 4\nu_s}{22\nu_f + 13\nu_s} (B-L) = \frac{28}{79} (B-L), \quad (7)$$

¹ The effects of density perturbations on baryon asymmetry is partially studied in Ref. [36], where the authors consider perturbations of the same order of magnitude as CMB and find the effect to be negligibly small. The present analysis is different from theirs in that we calculate the spatial average of the resulting baryon asymmetry, which should be the relevant quantity for the observed baryon asymmetry. Another difference is that we consider relatively large density perturbations, which we will find to have a net effect on the final averaged baryon abundance.

where $\nu_f = 3$ is the number of fermion generations and $\nu_s = 1$ is the number of Higgs doublets.

B. Prerequisites for cosmological perturbations

In an inhomogeneous universe, the time evolution of the right-handed neutrinos and baryon and/or lepton numbers occurs in the presence of cosmological perturbations. In this paper, we follow Refs. [43, 44] for the formulation of cosmological perturbations.

The background metric is given by the Friedmann-Lemaître-Robertson-Walker (FLRW) metric

$$ds^2 = g_{\mu\nu} dx^\mu dx^\nu = -dt^2 + a^2 \delta_{ij} dx^i dx^j, \quad (8)$$

where $g_{\mu\nu}$ is the metric tensor and $a = a(t)$ is the scale factor of the universe. We assume that the universe is radiation-dominated in the relevant epoch, and in this case the Friedmann equation is

$$3M_{\text{P}}^2 H^2 = \rho_r, \quad (9)$$

with

$$H = \frac{1}{2t}, \quad \rho_r = \frac{\pi^2}{30} g_* T^4. \quad (10)$$

Here $M_{\text{P}} = 1/\sqrt{8\pi G}$ is the reduced Planck mass, $H \equiv \dot{a}/a = a'/a^2$ is the Hubble parameter, and ρ_r is the radiation energy density. During the radiation-dominated epoch, the conformal time η defined by $d\eta = dt/a$ is related to the cosmological time as $\eta \propto t^{1/2}$. In what follows the dot denotes differentiation with respect to the physical time t , and the prime denotes differentiation with respect to the conformal time η .

The scalar perturbations of the metric tensor $g_{\mu\nu}$ are expressed in terms of four independent functions of time and space, A , B , C , and E , as [44]

$$g_{00} = -a^2(1 + 2A), \quad (11)$$

$$g_{0i} = -a^2 B_{,i}, \quad (12)$$

$$g_{ij} = a^2 \left[(1 + 2C) \delta_{ij} + 2 \left(E_{,ij} - \frac{1}{3} \delta_{ij} \nabla^2 E \right) \right]. \quad (13)$$

On the other hand, perturbation in the matter sector appears in the temperature fluctuation δT defined by

$$T = \bar{T} + \delta T, \quad \delta T \equiv \frac{\delta T}{\bar{T}}, \quad (14)$$

where \bar{T} is the spatially averaged temperature of the universe. With these definitions, it is useful to introduce new variables:

$$\bar{z} \equiv \frac{M_1}{\bar{T}}, \quad (15)$$

$$z_T \equiv \frac{M_1}{\bar{T} + \delta T} = \frac{\bar{z}}{1 + \delta T}. \quad (16)$$

In the following sections, we will use \bar{z} and z_T instead of physical time t and physical temperature T , respectively.

C. Boltzmann equation

The evolution of the number density of each particle species in the presence of collision processes is governed by the Boltzmann equation. After integrating over the momentum space, it takes the form (see Appendix B)

$$\mathcal{N}^\mu{}_{;\mu} = \frac{g_{\text{deg}}}{(2\pi)^3} \int \frac{d^3 p}{E} C[f], \quad (17)$$

where \mathcal{N}^μ is the number density current defined by $\mathcal{N}^\mu \equiv nU^\mu$ with n and U^μ being the number density and the 4-velocity, respectively, g_{deg} is the degrees of freedom of the species, f is the distribution function, and $C[f]$ is the collision term. The left-hand side of equation (17) can be written as

$$(nU^\mu)_{;\mu} = \bar{z} H (1 - A) \left(\frac{dn}{d\bar{z}} + \frac{3}{\bar{z}} n \right) + \frac{n}{a} (v^i{}_{,i} + 3C'), \quad (18)$$

where v^i is the 3-velocity, the latter of which is first order in perturbation. Here we used

$$U^0 = a^{-1}(1 - A), \quad U^i = a^{-1}v^i, \quad (19)$$

and equations (C1)–(C10).

For the right-handed neutrinos N_1 , we take only the decay and inverse decay into account. In this case, assuming that the right-handed neutrinos are in kinetic equilibrium, the thermal average of the right-hand side of equation (17) yields

$$\begin{aligned} & \left\langle \frac{g_{N_1}}{(2\pi)^3} \int \frac{d^3 p_{N_1}}{E_{N_1}} C \right\rangle \\ &= -\frac{4\pi^3 g_l g_\phi |\mathcal{M}|^2}{M_1} \cdot \frac{K_1(z_T)}{K_2(z_T)} \cdot [n_{N_1}(\bar{z}) - n_{N_1}^{\text{eq}}(z_T)] \\ &\equiv -\Gamma_D(\bar{z} = \infty) \left\langle \frac{1}{\gamma} \right\rangle (z_T) [n_{N_1}(\bar{z}) - n_{N_1}^{\text{eq}}(z_T)]. \quad (20) \end{aligned}$$

The collision term (20) is invariant under coordinate transformations: indeed, when the collision term is in the Local Inertial Frame Instantaneously at Rest with respect to the Comoving Observer (LIFIRCO), the cross sections have the same expressions as in the Minkowski space, and the collision term contains *no metric fluctuations* [45]. Any metric fluctuation is contained in, and arises from, the Liouville term, i.e., the left-hand side of equation (17). As a result, we obtain

$$\begin{aligned} & \left(\frac{dn_{N_1}}{d\bar{z}} + \frac{3}{\bar{z}} n_{N_1} \right) + \frac{n_{N_1}}{a\bar{z}H} (v^i{}_{,i} + 3C') \\ &\simeq -(1 + A) \frac{\Gamma_D(\bar{z} = \infty)}{\bar{z}H} \left\langle \frac{1}{\gamma} \right\rangle (z_T) [n_{N_1}(\bar{z}) - n_{N_1}^{\text{eq}}(z_T)] \\ &= -(1 + A) \bar{z} K \left\langle \frac{1}{\gamma} \right\rangle (z_T) [n_{N_1}(\bar{z}) - n_{N_1}^{\text{eq}}(z_T)], \quad (21) \end{aligned}$$

where $K \equiv \Gamma_D(\bar{z} = \infty)/\bar{z}^2 H$ is the so-called decay parameter. The evolution of the number density ratio

$N_{N_1} = n_{N_1}(\bar{z})/n_\gamma^{\text{eq}}(z_T)$ becomes

$$\frac{dN_{N_1}(\bar{z})}{d\bar{z}} = -(1+A)D(z_T)[N_{N_1}(\bar{z}) - N_{N_1}^{\text{eq}}(z_T)], \quad (22)$$

where

$$D(z_T) \equiv K\bar{z}\left\langle\frac{1}{\gamma}\right\rangle(z_T) = K\bar{z}\frac{K_1(z_T)}{K_2(z_T)}, \quad (23)$$

and

$$N_{N_1}^{\text{eq}}(z_T) = \frac{3}{8}z_T^2 K_2(z_T). \quad (24)$$

For N_{B-L} , the Liouville term is evaluated in the same way as before. The collision term contains the sourcing of lepton asymmetry from the CP asymmetry ε_1 through the difference between the non-equilibrium and equilibrium abundances of right-handed neutrinos. As a result, the evolution of N_{B-L} is governed by

$$\begin{aligned} \frac{dN_{B-L}(\bar{z})}{d\bar{z}} &= -\varepsilon_1(1+A)D(z_T)[N_{N_1}(\bar{z}) - N_{N_1}^{\text{eq}}(z_T)] \\ &\quad - (1+A)W_{\text{ID}}N_{B-L}, \end{aligned} \quad (25)$$

where

$$W_{\text{ID}}(z_T) = \frac{1}{4}K\bar{z}z_T^2 K_1(z_T), \quad (26)$$

is the washout factor without scattering [37].

To solve equations (22) and (25), we choose the conformal Newtonian gauge $A = \Psi$, $C = -\Phi$ and $B = E = 0$. The anisotropic stress is assumed to be negligible, and in this case $\Phi = \Psi$ holds. Equations (22) and (25) then respectively become

$$\frac{dN_{N_1}(\bar{z})}{d\bar{z}} = -(1+\Psi)D(z_T)[N_{N_1}(\bar{z}) - N_{N_1}^{\text{eq}}(z_T)], \quad (27)$$

and

$$\begin{aligned} \frac{dN_{B-L}(\bar{z})}{d\bar{z}} &= -\varepsilon_1(1+\Psi)D(z_T)[N_{N_1}(\bar{z}) - N_{N_1}^{\text{eq}}(z_T)] \\ &\quad - (1+\Psi)W_{\text{ID}}N_{B-L}. \end{aligned} \quad (28)$$

The time evolution of $\Psi = \Phi$ in a radiation dominated universe is given by [44]

$$\Psi(\eta, \mathbf{k}) = 2\mathcal{R}_i \frac{\sin \varphi - \varphi \cos \varphi}{\varphi^3}, \quad (29)$$

where \mathcal{R}_i is the primordial curvature perturbation in wavenumber space, and \mathbf{k} is the wavenumber with k being its absolute value. In a radiation-dominated epoch, φ is expressed as

$$\varphi = \frac{k\eta}{\sqrt{3}} \equiv \frac{\bar{z}}{\bar{z}_H}. \quad (30)$$

The parameter \bar{z}_H defined here can be regarded as specifying the time of horizon entry for each wavenumber.

Since $\Psi(\eta, \mathbf{x})$ is real, the Fourier transform can be written as

$$\begin{aligned} \Psi(\eta, \mathbf{x}) &= \int \frac{d^3k}{(2\pi)^3} e^{i\mathbf{k}\cdot\mathbf{x}} \Psi(\eta, \mathbf{k}) \\ &= \int \frac{d^3k}{(2\pi)^3} \frac{1}{2} [e^{i\mathbf{k}\cdot\mathbf{x}} \Psi(\eta, \mathbf{k}) + e^{-i\mathbf{k}\cdot\mathbf{x}} \Psi^*(\eta, \mathbf{k})] \\ &= \int \frac{d^3k}{(2\pi)^3} \left[2|\mathcal{R}_i| \cos \delta \frac{\sin \varphi - \varphi \cos \varphi}{\varphi^3} \right]. \end{aligned} \quad (31)$$

Here $\delta \equiv \delta' + \mathbf{k}\cdot\mathbf{x}$ is the phase of the perturbation with δ' being the complex phase of $\mathcal{R}_i = |\mathcal{R}_i| e^{i\delta'}$. Written this way, the time evolution of $\Psi = \Phi$ can be understood in terms of real functions only

$$\Psi(\eta, \mathbf{k}) = 2|\mathcal{R}_i| \cos \delta \frac{\sin \varphi - \varphi \cos \varphi}{\varphi^3}. \quad (32)$$

For each wavenumber \mathbf{k} , different values of the phase parameter δ can be regarded as specifying different spatial points. Since the final baryon asymmetry we observe is the spatial average, in our numerical analysis we take average of the final asymmetry with respect to the phase δ .

The temperature fluctuation δ_T is related to the fluctuation in the radiation energy density δ_r as

$$\delta_r = \frac{\delta\rho_r}{\bar{\rho}} = 4\frac{\delta T}{T} = 4\delta_T. \quad (33)$$

The evolution of δ_r is given by [44]

$$\delta_r = -\frac{2}{3}(k\eta)^2 \Psi - 2\eta\Psi' - 2\Psi, \quad (34)$$

where we used $\Psi = \Phi$. Substituting equation (32) into equation (34), we obtain

$$\delta_r = 8|\mathcal{R}_i| \cos \delta \frac{\sin \varphi - \varphi \cos \varphi - \varphi^2 \sin \varphi + \frac{1}{2}\varphi^3 \cos \varphi}{\varphi^3}, \quad (35)$$

and correspondingly

$$\delta_T = 2|\mathcal{R}_i| \cos \delta \frac{\sin \varphi - \varphi \cos \varphi - \varphi^2 \sin \varphi + \frac{1}{2}\varphi^3 \cos \varphi}{\varphi^3}. \quad (36)$$

D. Neutrino mass parameters

In our setup, the amount of baryon asymmetry depends on the heavy neutrino mass M_1 , the decay parameter K , and the degree of CP asymmetry ε_1 . M_1 determines the temperature at which the abundance of N_1 starts to decline. K determines the time (or, the value of \bar{z}) when N_1 decouples from the thermal bath. ε_1 controls the efficiency of the generation of $B-L$ via N_1 decay. The latter two parameters K and ε_1 depend on the neutrino masses, Yukawa couplings, and other parameters in

the Lagrangian. In this subsection, we introduce various neutrino mass parameters that are useful to interpret the results (see, e.g., Ref. [37] for details).

The masses of light neutrinos are denoted by m_1 , m_2 , and m_3 ($m_1 < m_2 < m_3$). The *effective neutrino mass* is defined by

$$\tilde{m}_1 \equiv \frac{(m_D^\dagger m_D)_{11}}{M_1}, \quad (37)$$

where $(m_D)_{\alpha\beta} = y_{\alpha\beta}v$ with $v \simeq 174$ GeV being the Higgs vacuum expectation value (VEV). The decay parameter K is proportional to \tilde{m}_1 :

$$K \equiv \frac{\tilde{m}_1}{m_*}, \quad m_* = \sqrt{\frac{64\pi^3 g_*}{45}} \frac{v^2}{M_P} \simeq 1.08 \times 10^{-3} \text{ eV}, \quad (38)$$

where $g_* = 106.75$ is the number of degrees of freedom in the SM. For instance, $K = 0.01, 1, 100$ corresponds to $\tilde{m}_1 \simeq 10^{-5}, 10^{-3}, 10^{-1}$ eV, respectively. The two regimes $\tilde{m}_1 > m_*$ and $\tilde{m}_1 < m_*$ are referred to as the *strong washout* and *weak washout* regimes, respectively [37]. Note that \tilde{m}_1 must lie in the range of $m_1 \leq \tilde{m}_1 \lesssim m_3$ [46].

The Yukawa coupling has an upper bound from perturbativity, which in turn imposes a corresponding upper limit on the absolute value of the CP asymmetry. The maximal absolute CP asymmetry is given by (see Appendix E)

$$|\varepsilon_1|^{\max} = \frac{3}{16\pi} \frac{M_1 m_3}{v^2} \left[1 - \frac{m_1}{m_3} \left(1 + \frac{m_3^2 - m_1^2}{\tilde{m}_1^2} \right)^{1/2} \right]. \quad (39)$$

In this paper, we use the maximum value of the CP asymmetry (39) for $|\varepsilon_1|$ to calculate the maximum baryon-to-photon ratio η_b^{\max} .

In the subsequent section, we compute the evolution of N_{N_1} and N_{B-L} for given M_1 , K , and ε_1 . Then we map the result to the (\tilde{m}_1, M_1) plane and discuss the allowed region, where the generated $B-L$ asymmetry is large enough to explain the observed baryon asymmetry. Since entropy injection may occur after the production of asymmetry, we only require that the baryon asymmetry exceed the observed value. For the latter we use the result from the Planck collaboration [10]

$$\eta_b^{\text{CMB}} = (6.144 \pm 0.038) \times 10^{-10}, \quad (40)$$

and require $\eta_b^{\max} \geq (\eta_b^{\text{CMB}})_{\text{low}}$, where

$$(\eta_b^{\text{CMB}})_{\text{low}} = 6.0 \times 10^{-10}, \quad (41)$$

is the 3σ lower limit.

Another useful mass is the *absolute mass scale* defined by

$$\bar{m} = \sqrt{m_1^2 + m_2^2 + m_3^2}. \quad (42)$$

As discussed in Ref. [46], the allowed region on the (\tilde{m}_1, M_1) plane shrinks with increasing \bar{m} because the lower limit of \tilde{m}_1 increases, as we sketch below.

The value of \bar{m} can be inferred from the mass measurements of neutrino oscillation experiments and cosmological observations. Given the neutrino mass patterns, i.e., either $m_3^2 - m_2^2 > m_2^2 - m_1^2$ or $m_3^2 - m_2^2 < m_2^2 - m_1^2$, the dependence of m_3 on m_1 is fixed. In this paper we analyze the normal hierarchy $m_1 < m_2 < m_3$ only. In this case, the relations $m_3^2 - m_2^2 = \Delta m_{\text{atm}}^2$ and $m_2^2 - m_1^2 = \Delta m_{\text{sol}}^2$ lead to

$$\begin{aligned} m_3^2 &= m_1^2 + \Delta m_{\text{atm}}^2 + \Delta m_{\text{sol}}^2, \\ m_2^2 &= m_1^2 + \Delta m_{\text{sol}}^2, \\ \bar{m}^2 &= 3m_1^2 + \Delta m_{\text{atm}}^2 + 2\Delta m_{\text{sol}}^2. \end{aligned} \quad (43)$$

These relations can be rewritten as

$$\begin{aligned} m_1^2 &= \frac{1}{3}(\bar{m}^2 - \Delta m_{\text{atm}}^2 - 2\Delta m_{\text{sol}}^2), \\ m_2^2 &= \frac{1}{3}(\bar{m}^2 - \Delta m_{\text{atm}}^2 + \Delta m_{\text{sol}}^2), \\ m_3^2 &= \frac{1}{3}(\bar{m}^2 + 2\Delta m_{\text{atm}}^2 + \Delta m_{\text{sol}}^2). \end{aligned} \quad (44)$$

According to the neutrino oscillation experiments (see Ref. [47] and references therein), the mass differences are known to be

$$\begin{aligned} \Delta m_{\text{atm}}^2 &= (2.453 \pm 0.033) \times 10^{-3} \text{ eV}^2, \\ \Delta m_{\text{sol}}^2 &= (7.53 \pm 0.18) \times 10^{-5} \text{ eV}^2. \end{aligned} \quad (45)$$

Thus \bar{m} takes its minimum value

$$\bar{m} = \sqrt{\Delta m_{\text{atm}}^2 + 2\Delta m_{\text{sol}}^2} \simeq 0.051 \text{ eV}, \quad (46)$$

for $m_1 = 0$. Furthermore, CMB observations together with baryon acoustic oscillation (BAO) measurements constrain the sum of the mass eigenvalues of light neutrinos from above as [11]

$$m_1 + m_2 + m_3 < 0.13 \text{ eV} \quad (47)$$

at the 2σ level. Substituting equation (44) and using equation (45), we find

$$\bar{m} < 0.078 \text{ eV}. \quad (48)$$

This upper limit is more relaxed when CMB alone is used without BAO [10]

$$m_1 + m_2 + m_3 < 0.26 \text{ eV} \quad (49)$$

at the 2σ level. In this case, we obtain

$$\bar{m} < 0.15 \text{ eV}. \quad (50)$$

In the following we present the allowed regions in the (\tilde{m}_1, M_1) plane for the lower limit on \bar{m} (46), the two types of upper limits (48) and (50), and also $\bar{m} = \bar{m}_{\max} \equiv 0.19$ eV, the last of which corresponds to the value just before the allowed region disappears when scattering is taken into account.

III. IMPLICATIONS TO LEPTOGENESIS

A. Intuitive picture

Before proceeding to the numerical results, we describe the qualitative behavior of the evolution of right-handed neutrinos in the presence of density perturbations. When the right-handed neutrinos decouple from the thermal bath at temperature T , the equilibrium abundance of right-handed neutrinos N_1 can be approximated by the Boltzmann distribution

$$N_{N_1}^{\text{eq}} \sim \exp\left(-\frac{M_1}{T}\right). \quad (51)$$

Substituting equation (14) into (51), $N_{N_1}^{\text{eq}}$ behaves as

$$N_{N_1}^{\text{eq}} \sim \exp\left(-\frac{M_1}{\bar{T}}\right) \exp\left(\frac{M_1}{\bar{T}} \delta_T\right). \quad (52)$$

Therefore, if the temperature fluctuation is sufficiently large

$$\delta_T \gtrsim \frac{\bar{T}}{M_1}, \quad (53)$$

the linear expansion of $\exp(M_1 \delta_T / \bar{T})$ causes a significant error. For the strong washout regime, the actual abundance N_{N_1} closely follows this equilibrium abundance, and hence the linear approximation also breaks down for N_{N_1} . The condition (53) translates to $\delta_T \gtrsim 0.05$ given that the freeze-out of $|N_{B-L}|$ occurs at $\bar{z} = M_1 / \bar{T} \sim 10 - 20$.

If we linearize with respect to δ_T , the baryon number would never increase because the average over the phase δ will cancel out the contributions from positive δ_T and those from negative δ_T . Therefore, the increase in the baryon number (Figure 2) represents a *beyond-linear* effect related to δ_T , which we call ‘‘acoustically driven freeze-out.’’

B. Time evolution of N_1 and $B - L$

Figure 1 compares the time evolutions of the abundance of the right-handed neutrino N_{N_1} and the baryon-minus-lepton number N_{B-L} in the presence (thick lines) and absence (thin lines) of perturbations. The decay parameter $K = \tilde{\Gamma}_D / \bar{z}^2 H$ is taken to be 100, 1, and 0.01 from top to bottom. The curvature perturbation is set to $|\mathcal{R}_i| = 0.2$ and the phase is chosen to $\delta = \pi$ that corresponds to a specific spatial point. Also, a monochromatic wave $\bar{z}_H = 1$ is assumed, corresponding to the horizon re-entry somewhat before the freeze-out of $|N_{B-L}|$. For the time evolution with other values of $\bar{z}_H = 1$, see Appendix A. Also, for more realistic density fluctuations described by a superposition of monochromatic waves, see the discussion in Section IV.

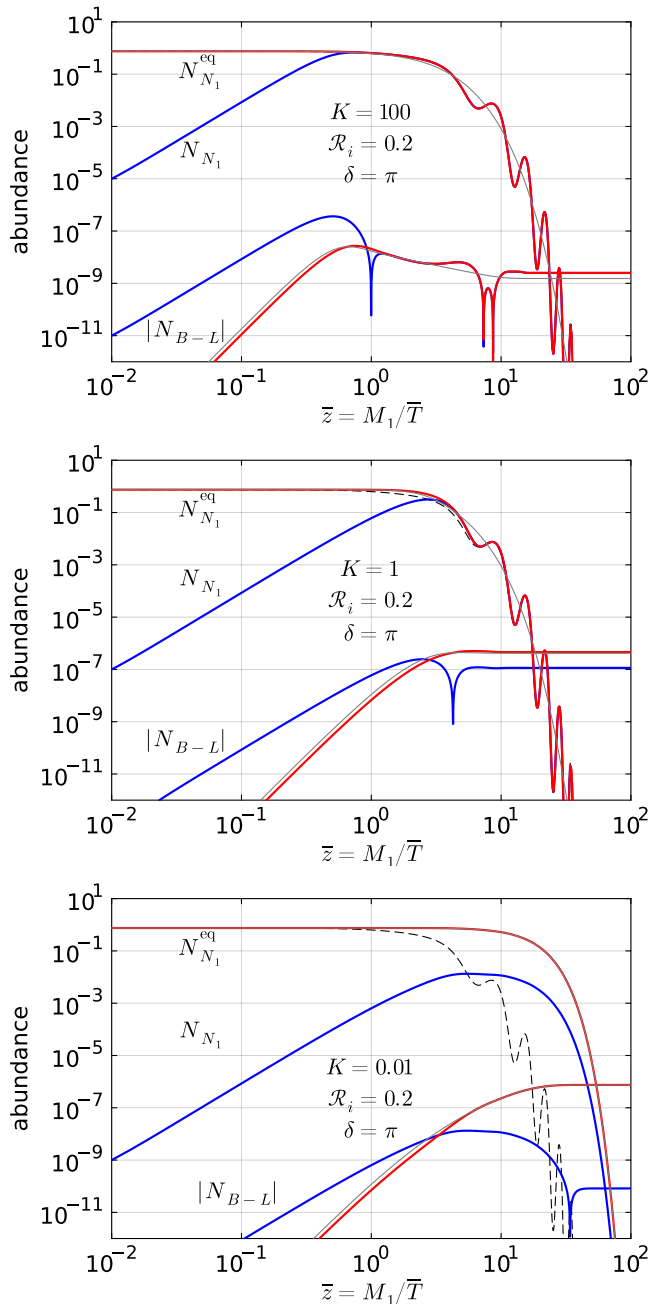


FIG. 1. *Top*: evolution of the abundance of right-handed neutrinos N_{N_1} and the absolute value of the baryon-minus-lepton number $|N_{B-L}|$ for the decay parameter $K = 100$, the amplitude of primordial curvature perturbation $|\mathcal{R}_i| = 0.2$, and the phase $\delta = \pi$. The red and blue curves show the thermal and zero initial abundances for N_{N_1} , respectively. These curves merge into a single curve at later times. The thin gray curves depict the results for $|\mathcal{R}_i| = 0$ with the thermal initial abundance. The dashed line represents the equilibrium number density of right-handed neutrinos $N_{N_1}^{\text{eq}}$. *Middle*: same as the top panel but for the decay parameter $K = 1$. *Bottom*: same as the top panel but for the decay parameter $K = 0.01$.

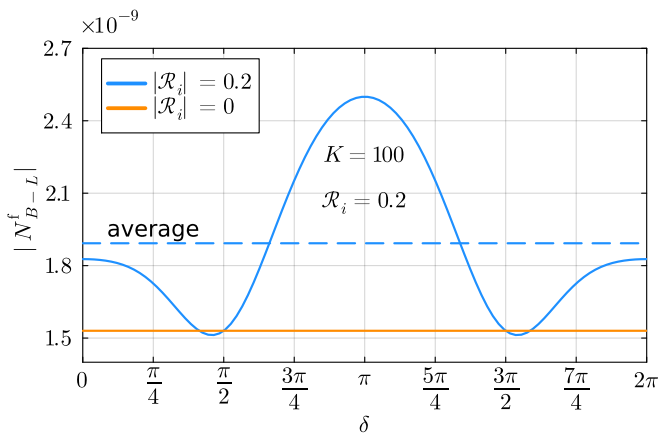


FIG. 2. Baryon-minus-lepton number $|N_{B-L}|$ after freeze-out, denoted by $|N_{B-L}^f|$, for different values of δ . The blue solid curve shows the result with temperature fluctuations, while the orange solid line shows that without fluctuations. In the presence of perturbations, temperature oscillations at different spatial locations have different values for the phase δ , resulting in the difference in $|N_{B-L}^f|$ at different spatial points. Averaging this over δ yields the spatial average shown by the blue dashed line, which is found to be greater than the value without perturbations. Here the zero initial abundance is assumed for N_{N_1} , but the result with the thermal initial abundance is almost the same.

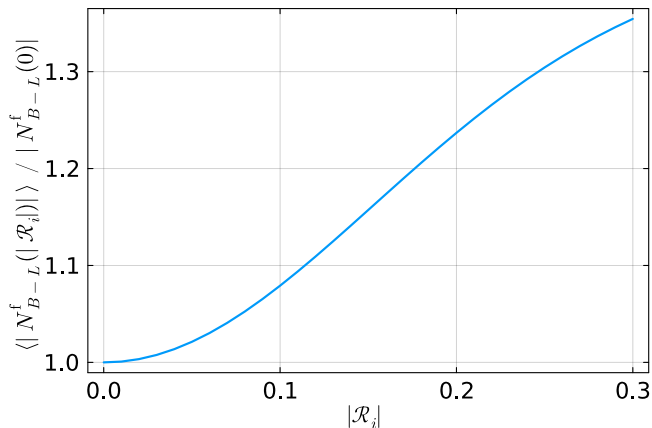


FIG. 3. Ratio between the spatially averaged freeze-out value $\langle |N_{B-L}^f| \rangle_{\text{space}}$ with and without perturbations, as a function of the amplitude of the primordial curvature perturbation $|\mathcal{R}_i|$.

In the top panel of Figure 1 ($K = 100$), the actual and equilibrium abundances of right-handed neutrinos N_{N_1} and $N_{N_1}^{\text{eq}}$ oscillate significantly for $\bar{z} \gtrsim \mathcal{O}(1)$. As a result, $|N_{B-L}|$ also oscillates around $\bar{z} \sim 10$, leading to the increase in the value of $|N_{B-L}|$ after the freeze-out denoted by $|N_{B-L}^f|$. This increase occurs for both initial conditions $N_{N_1} = 3/4$ or $N_{N_1} = 0$. On a closer look, we observe that the freeze-out value $|N_{B-L}^f|$ is determined by the downstroke of the temperature and of the corresponding equilibrium value $N_{N_1}^{\text{eq}}$ around $\bar{z} \simeq 15$. For this

parameter point, the freeze-out is dominantly driven by the sudden decrease in the temperature caused by sound waves, not by the slow decrease in the average temperature. Of course, different spatial points have different oscillation phases, and thus we have to take average over the phase δ as performed below.

In the middle panel of Figure 1 ($K = 1$), we still observe oscillations in the abundance of right-handed neutrinos N_{N_1} and its equilibrium value $N_{N_1}^{\text{eq}}$. The freeze-out value $|N_{B-L}^f|$ is thus enhanced in the same way as the top panel, though the enhancement is smaller. Such enhancement is observed for the strong washout regime $1 \leq K \leq 100$. For the weak washout regime $K < 1$, in contrast, N_{N_1} does not oscillate any more and the freeze-out value $|N_{B-L}^f|$ is almost identical to the case without perturbations, as seen from the bottom panel of Figure 1 ($K = 0.01$). This tendency is simply because N_{N_1} is not tightly coupled with $N_{N_1}^{\text{eq}}$ any more and thus the oscillations do not play any role in this parameter range.

To evaluate the effect of density fluctuations on the final baryon asymmetry, the freeze-out value $|N_{B-L}^f|$ must be averaged over different values of δ . Figure 2 depicts the freeze-out value $|N_{B-L}^f|$ as a function of δ . Interestingly, the freeze-out value $|N_{B-L}^f|$ is found to increase for almost all values of δ . This is because, oscillations that happen with the “right phase” boost the freeze-out of N_{N_1} and N_{B-L} as seen in the top panel of Figure 1, while oscillations with the “wrong phase” (i.e., oscillations that increase the temperature around $\bar{z} \simeq 15$) simply push the system back to equilibrium again, resulting in the system waiting for the freeze-out that occurs on the next occasion of temperature decrease. Thus the “wrong phase” does not lead to the decrease in the freeze-out value.

Based on these observations, we compare the spatially averaged value $\langle |N_{B-L}^f| \rangle_{\text{space}}$ with the freeze-out value in the absence of fluctuations. We find

$$\frac{\langle |N_{B-L}^f| \rangle_{\text{space}}(|\mathcal{R}_i| = 0.2)}{|N_{B-L}^f|(|\mathcal{R}_i| = 0)} \sim 1.25. \quad (54)$$

for the parameter point $|\mathcal{R}_i| = 0.2$ and $\bar{z}_H = 1$, as seen from Figure 2. We emphasize that the ratio is greater than unity, because the increase in $|N_{B-L}^f|$ for the phase $\delta \sim \pi$ is not canceled out by the contribution from $\delta \sim 0$ due to the reason explained just above. This enhancement would vanish if one linearizes the system in the temperature fluctuation δ_T , and therefore this effect is a beyond-linear effect, which might be called “acoustically enhanced freeze-out.”

In Figure 3 we plot the ratio between the spatially averaged freeze-out value $\langle |N_{B-L}^f| \rangle_{\text{space}}(|\mathcal{R}_i|)$ and the freeze-out value without fluctuations as a function of the primordial curvature perturbation $|\mathcal{R}_i|$. We find that the ratio exceeds unity for any $|\mathcal{R}_i| > 0$, and that it increases monotonically for $0 \leq |\mathcal{R}_i| \lesssim 0.3$. Figures with other values of \bar{z}_H are shown in Appendix A.

C. Parameter regions for successful leptogenesis

Figure 4 shows the parameter regions for successful leptogenesis on the (\tilde{m}_1, M_1) plane. For a given value of \bar{m} , there are two curves with (blue) and without (orange) density fluctuations. The primordial curvature perturbation is taken to be $|\mathcal{R}_i| = 0.2$. In the region above each curve, the produced amount of baryons exceeds the lower limit given by the CMB data (40). In the previous subsection, we considered the case of $K = 100, 1$, and 0.01 corresponding to $\tilde{m}_1 \simeq 0.1, 10^{-3}$, and 10^{-5} eV, respectively. While the contours are not closed in this plot, it is known that upper limits on M_1 arise once $\Delta L = 2$ scatterings are taken into account (see e.g., Ref. [37]). The reason we do not take account of these scatterings is simply to illustrate the effect of acoustically driven freeze-out in the simplest setup (see also discussion in Section IV).

In the case of $m_1 = 0$, the absolute mass (42) takes its minimum value $\bar{m} = 0.051$ eV. The resulting constraint is shown in the solid lines. In the weak washout regime $\tilde{m}_1 \lesssim 10^{-3}$ eV, the constraint with temperature fluctuations is almost identical to the one without temperature fluctuations. In the strong washout regime $\tilde{m}_1 \gtrsim 10^{-3}$ eV, the allowed region with fluctuations gets slightly extended from that without fluctuations due to the enhancement by the acoustically driven freeze-out.

The allowed parameter space shrinks as \bar{m} increases, as discussed in Ref. [46]. For instance, in the case of $\bar{m} = 0.078$ eV, the region for $\tilde{m}_1 \gtrsim 0.03$ eV is ruled out as shown in the dot-dashed lines. As in the case of $\bar{m} = 0.051$ eV, including fluctuations enlarges the allowed region. Similar behavior is observed for $\bar{m} = 0.15$ eV (dashed lines) and $\bar{m}_{\max} = 0.19$ eV (dot-dot-dashed lines).

We thus conclude that the beyond-linear effect can enlarge the parameter space for successful leptogenesis if the amplitudes of primordial density fluctuations are sufficiently large. The effect of perturbations is important in the strong washout regime

$$8.7 \times 10^{-3} \text{ eV} \lesssim \tilde{m}_1 \lesssim 5.0 \times 10^{-2} \text{ eV}. \quad (55)$$

The dependence on the primordial curvature perturbation $|\mathcal{R}_i|$ can be inferred from Figure 3. Note that the neutrino oscillation experiments suggest that the masses of light neutrinos likely lie in this range, see equation (45). In the future, as neutrinoless double beta decay experiments such as CANDLES [48], CUORE [49], EXO [50], KamLAND-Zen [51], LEGEND [52], NEMO-3 and SuperNEMO [53, 54] (see also Ref. [24] and references therein) achieve better sensitivities, not only will the upper limits on the mass eigenvalues of the light neutrinos improve, but the absolute mass scale \bar{m} may finally be determined. If the determined mass scale falls within the ballpark of $\bar{m} \gtrsim 0.1$ eV, the effect discussed in the present paper turns out to be relevant, as seen from Figure 4.

IV. DISCUSSION AND CONCLUSIONS

In this paper, we studied the effect of primordial density fluctuations on the freeze-out of heavy particles. Primordial density fluctuations within the Hubble horizon propagate as sound waves during the freeze-out of these particles. Sound waves cause temperature oscillation at each spatial point, driving oscillation in the abundance of massive particles with respect to radiation. Using leptogenesis as an illustrative framework, we have derived the governing equations that describe the evolution of these heavy particles in the presence of fluctuations, and found that the exponential dependence of the abundance of heavy particles on the local temperature causes a beyond-linear effect in the system, see equations (51) and (52).

As a proof of concept, we applied the formulation to the scenario of vanilla leptogenesis and demonstrated how temperature fluctuations affect the abundance of the right-handed neutrino and the resulting $B - L$ asymmetry. We indeed observed oscillations in the equilibrium abundance of the right-handed neutrino N_1 and in the baryon-minus-lepton number N_{B-L} (Figure 2). Interestingly, the density fluctuations always increase the final baryon-to-photon ratio compared to the case without fluctuations, even after taking spatial average (Figure 3). This suggests that the effect of oscillations cannot be captured within linear perturbation. Qualitatively, the equilibrium value of the right-handed neutrino is governed by the Boltzmann factor $\exp(-E/T) \simeq \exp(-E/\bar{T}) \exp(E\delta T/\bar{T}^2)$, and the fast temperature oscillation makes it harder for the non-equilibrium abundance of N_1 to follow this equilibrium value. If the temperature oscillation occurs with the right phase, the freeze-out of N_1 is dominantly driven by the oscillation, not by the slow decrease in the average temperature, and the resulting $|N_{B-L}|$ is enhanced (top panel of Figure 3, around $\bar{z} \simeq 15$). We call this effect ‘‘acoustically driven freeze-out’’. Of course, each spatial point has its own oscillation phase, and thus the enhancement in $|N_{B-L}|$ does not occur uniformly. However, the exponential enhancement of $|N_{B-L}|$ in some regions cannot be fully canceled out by the contributions from other regions. As a result, we get a net enhancement of the baryon asymmetry even after spatial average.

From the consideration above, the allowed parameter space for leptogenesis gets enlarged in the presence of fluctuations. We presented the allowed regions $\eta_b \geq (\eta_b^{\text{CMB}})_{\text{low}}$ in the (\tilde{m}_1, M_1) plane for a given absolute neutrino mass scale $\bar{m} = \sqrt{m_1^2 + m_2^2 + m_3^2}$ (Figure 4). The effective neutrino mass \tilde{m}_1 is linearly proportional to the decay parameter K and thus characterizes the weak and strong washout regimes (Figure 4, $\tilde{m} \lesssim 10^{-3}$ eV and $\tilde{m} \gtrsim 10^{-3}$ eV, respectively). When temperature fluctuations are included, we indeed found an enlarged allowed regions. The difference arises mainly in the strong washout regime, because in the weak washout regime the actual N_1 abundance is almost unaffected by

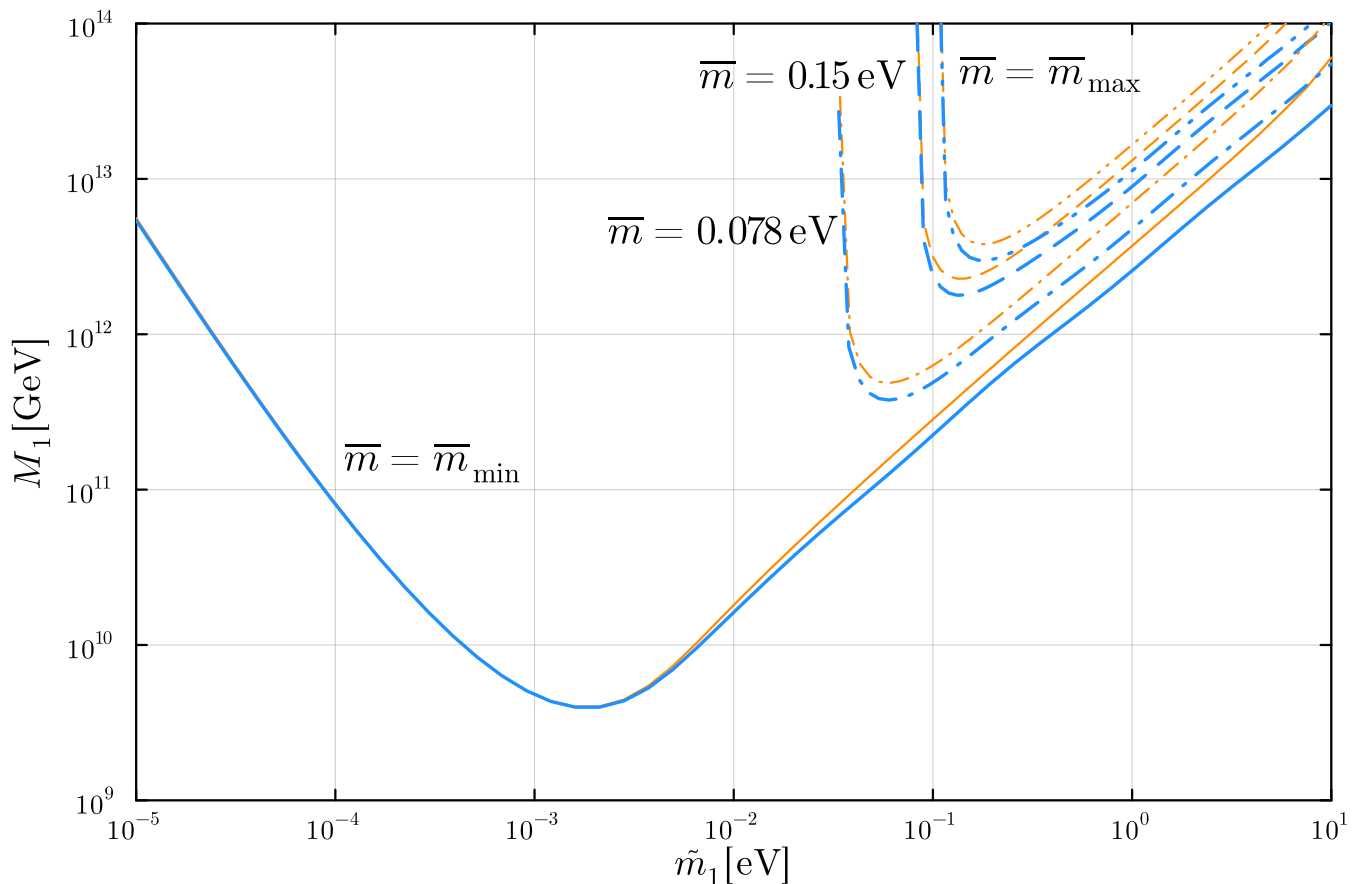


FIG. 4. Allowed regions for successful leptogenesis. The normal hierarchy and zero initial abundance for N_{N_1} are assumed. The curves show (\tilde{m}_1, M_1) where $\eta_b^{\max} = (\eta_b^{\text{CMB}})_{\text{low}} = 6.0 \times 10^{-10}$ is satisfied for $\bar{m} = (0.051, 0.078, 0.15, 0.19)$ eV. For a given \bar{m} , the region above the curves is the one for successful leptogenesis. The blue and orange curves represent the case with and without temperature fluctuations δ_T , respectively. The primordial curvature perturbation is taken to be $|\mathcal{R}_i| = 0.2$. We can see that the allowed region in (\tilde{m}_1, M_1) is expanded by the effect of δ_T . The solid lines correspond to $m_1 = 0$ such that $\bar{m} = \bar{m}_{\min} = 0.051$ eV. The dash-dot lines are for $\bar{m} = 0.078$ eV, corresponding to the upper limit from CMB and BAO observations [11]. The dashed lines are for $\bar{m} = 0.15$ eV, corresponding to the upper limit from CMB alone [10]. The dot-dot-dashed lines correspond to $\bar{m} = 0.19$ eV. If scatterings are included, the upper boundary appears, and the allowed region would disappear for $\bar{m} > 0.19$ eV [46].

its oscillating equilibrium value (bottom panel of Figure 3). While the quantitative difference is not dramatically large, given that the neutrino oscillation experiments point toward the strong washout regime [47], our findings will be relevant when we find relatively large \bar{m} from cosmological observations [10, 11].

We conclude by mentioning several possible future directions. For the microphysics side, we took only decay and inverse decay into account in this study. However, it is well known that $\Delta L = 2$ scattering imposes an (\bar{m} -dependent) upper bound on M_1 and thus closes the allowed region in the (M_1, \tilde{m}_1) plane [46]. Such scattering processes will not bring qualitative changes in the behavior of acoustically driven freeze-out since they do not affect the oscillating equilibrium abundance itself, which is the main reason for the net enhancement in the asymmetry. Nevertheless, identifying the allowed parameter

space including all the known microphysical effect will be important in preparing for future precision measurements. For the macrophysics side, in this paper we injected monochromatic sound waves for simplicity. In reality, however, fluctuations are a superposition of waves with various wavenumbers characterized by the power spectrum of the primordial curvature perturbation. Thus the effect of fluctuations on freeze-out will ultimately be described by the power spectrum, and it would be interesting to construct analytical formulations for it. In addition, it has been pointed that the sound waves can evolve to shock waves in the long run [55]. Shock waves by definition have discontinuities in thermodynamic parameters and hence are expected to enhance the sudden freeze-out of heavy particles. Incorporating all these aspects will be important and interesting future steps, to which we will come back elsewhere.

ACKNOWLEDGMENTS

The work of K.H. is supported by the JST FOREST Program (JPMJFR2136) and the JSPS Grant-in-Aid for Scientific Research (20H05639, 20H00158, 23H01169, 23H04900). The work of R.J. is supported by JSPS KAKENHI Grant Numbers 23K17687, 23K19048, and 24K07013.

Appendix A: Time evolution for different values of \bar{z}_H

In this Appendix, we plot the time evolution of N_1 and $B-L$, the freeze-out values of $B-L$, and their dependence on $|\mathcal{R}_i|$ for $\bar{z}_H = 0.5$ and 2.

Figures 5 and 6 show the time evolution of N_1 and $B-L$, Figures 7 and 8 show the freeze-out values of $B-L$, and Figures 9 and 10 show the dependence on $|\mathcal{R}_i|$ for $\bar{z}_H = 0.5$ and 2. These figures correspond to Figures 1–3 in the main text, in which $\bar{z}_H = 1$ is adopted.

Appendix B: Derivation of the Boltzmann equation

1. The Boltzmann equation

We begin with the Boltzmann equation [45]:

$$\frac{df}{d\lambda} = C[f] \quad \Rightarrow \quad P^0 \frac{df}{d\eta} = C[f], \quad (\text{B1})$$

where f is the distribution function, λ is the affine parameter, $C[f]$ is the collision term, and P^0 is the zeroth component of the energy-momentum 4-vector P^μ . We integrate the former equation using the integral measure in momentum space defined as

$$\pi = g_{\text{deg}} \frac{d^3 p}{E}, \quad (\text{B2})$$

where g_{deg} represents the internal degrees of freedom of the species, and E and p^i are the energy and 3-momentum of the particle evaluated in the local inertial frame, respectively.

2. Equivalence of integral measures

The integral measure (B2) evaluated in an arbitrary coordinate system is given by [45]

$$\pi \equiv g_{\text{deg}} \frac{\sqrt{-g} d^3 P}{P_0} = g_{\text{deg}} \frac{d^3 P}{P^0 \sqrt{-g}}. \quad (\text{B3})$$

To check this, note that the relation between the 4-momenta evaluated in the general coordinate system and in the local inertial system is

$$P^\mu = e^\mu_{\nu'} p^{\nu'}, \quad (\text{B4})$$

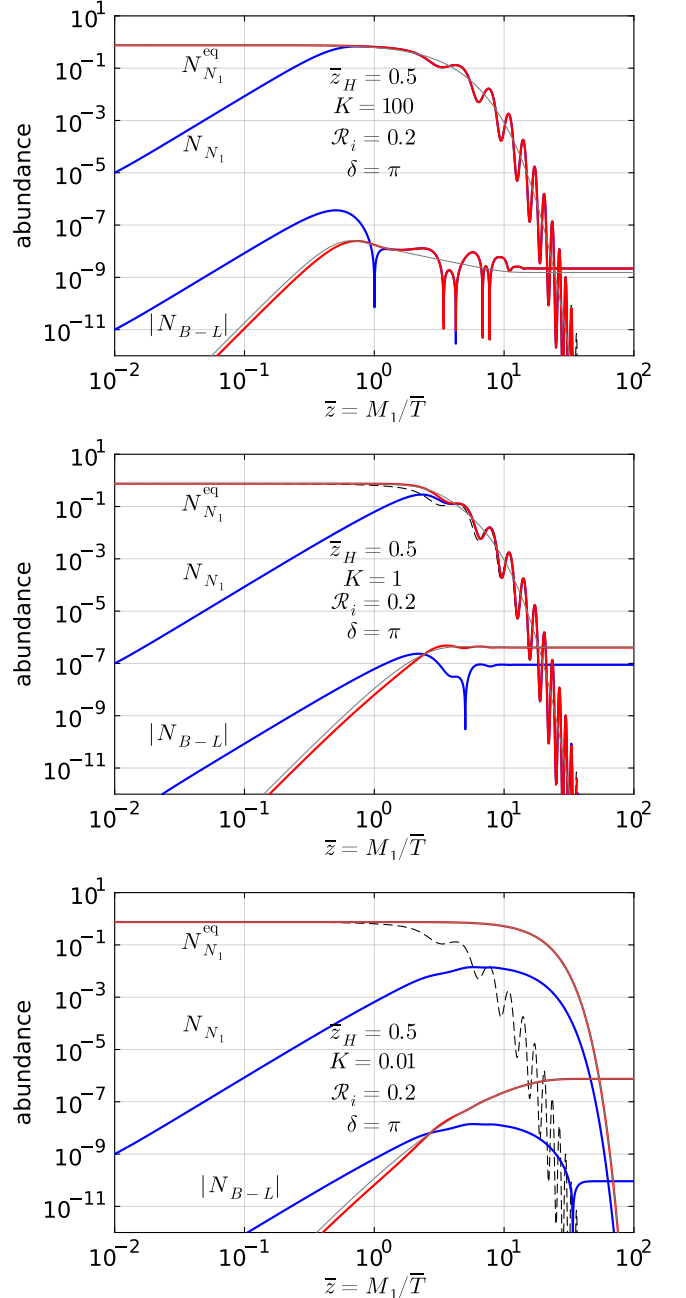


FIG. 5. Time evolution of N_{N_1} and $|N_{B-L}|$. Parameter values are the same as Figure 1 except for $\bar{z}_H = 0.5$.

where $e^\mu_{\nu'}$ is the tetrad, and $p^0 = -p_0 = E$ is the instantaneous energy of the particle with respect to the local observer. The tetrad satisfies $e^\mu_{\alpha'} e^{\nu'}_{\beta'} g_{\mu\nu} = \eta_{\alpha'\beta'}$. Using (B4) and $E dE = p_j dp^j$, we may rewrite dP as

$$\begin{aligned} dP^i &= e^i_0 \frac{\partial p^0}{\partial p^j} dp^j + e^i_k \frac{\partial p^k}{\partial p^j} dp^j \\ &= e^i_0 \frac{p^j}{E} dp^j + e^i_j dp^j = \left(e^i_0 \frac{p^j}{E} + e^i_j \right) dp^j. \end{aligned} \quad (\text{B5})$$

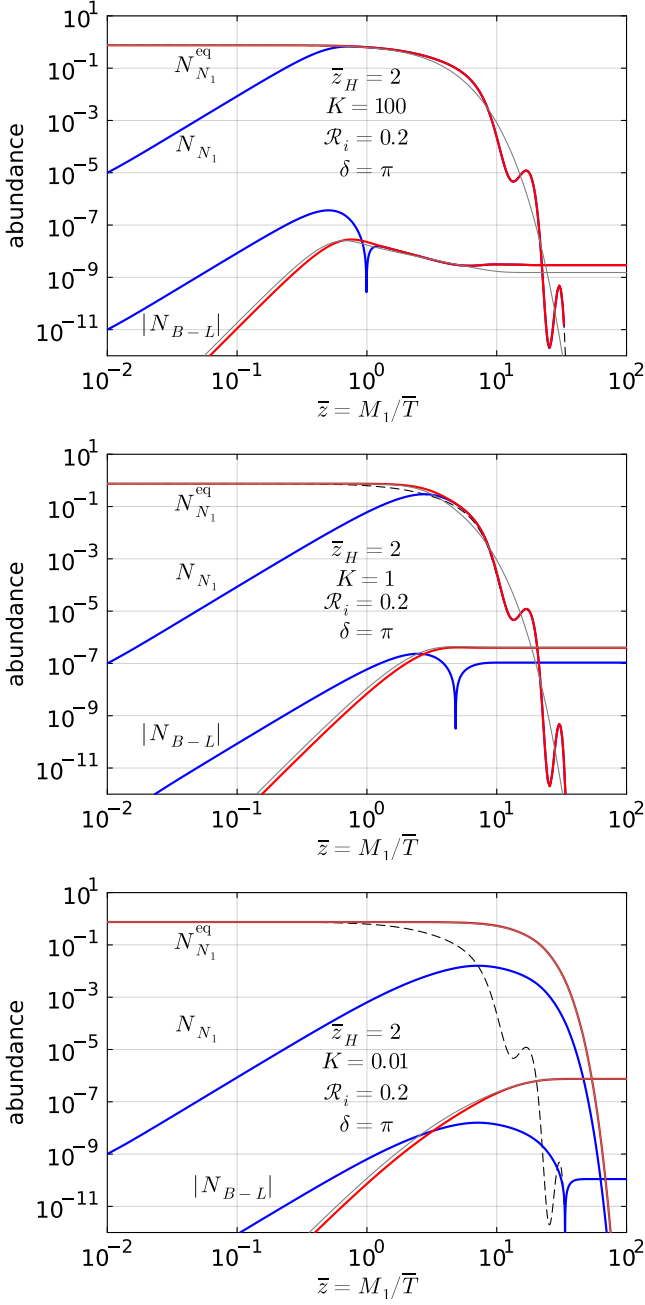


FIG. 6. Time evolution of N_{N_1} and $|N_{B-L}|$. Parameter values are the same as Figure 1 except for $\bar{z}_H = 2$.

Substituting this into dP in (B3) and using

$$P_0 = g_{0\mu} e^{\mu}{}_{\nu'} p^{\nu'} = \eta_{\nu'\sigma'} (e^{-1})^{\sigma'}{}_{\rho} p^{\rho}, \quad (\text{B6})$$

the integral measure indeed reduces to

$$\pi = g_{\text{deg}} \frac{d^3 p}{E}. \quad (\text{B7})$$

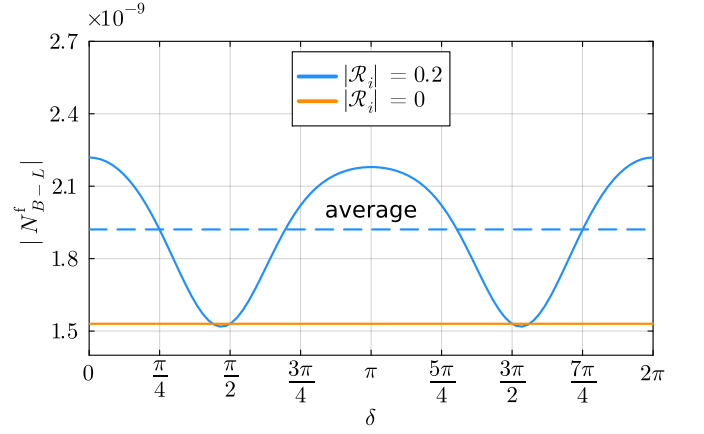


FIG. 7. Freeze-out value of $|N_{B-L}|$ for different values of δ . Parameter values are the same as Figure 2 except for $\bar{z}_H = 0.5$.

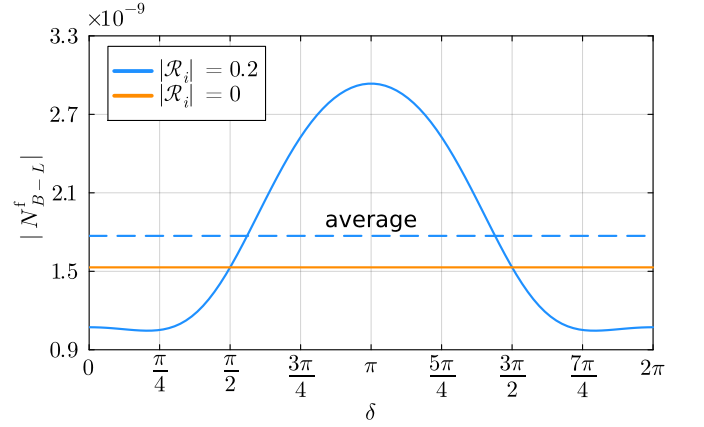


FIG. 8. Freeze-out value of $|N_{B-L}|$ for different values of δ . Parameter values are the same as Figure 2 except for $\bar{z}_H = 2$.

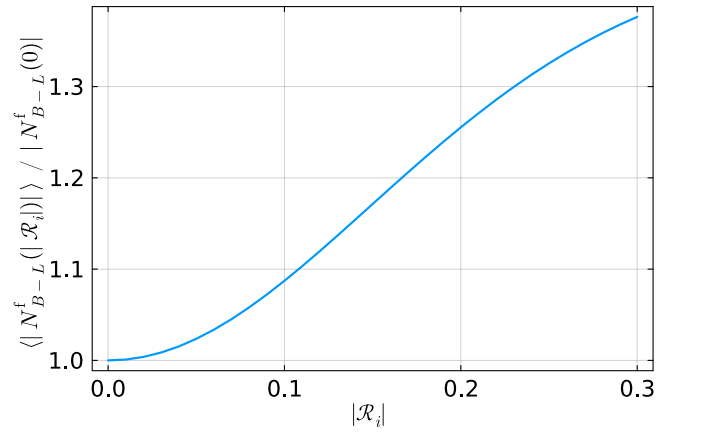


FIG. 9. Ratio between the spatially averaged freeze-out value $\langle |N_{B-L}^f| \rangle_{\text{space}}$ with and without perturbations. Parameter values are the same as Figure 3 except for $\bar{z}_H = 0.5$.

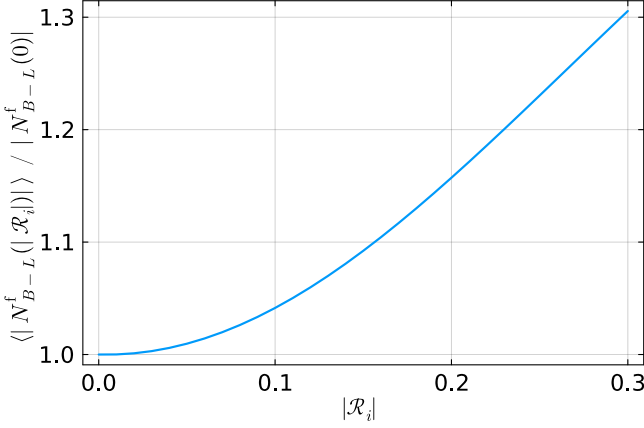


FIG. 10. Ratio between the spatially averaged freeze-out value $\langle |N_{B-L}^f| \rangle_{\text{space}}$ with and without perturbations. Parameter values are the same as Figure 3 except for $\bar{z}_H = 2$.

3. Equivalence of (17) and the integral of (B1)

In this subsection we show the equivalence of equation (17) and the integral of (B1) following Ref. [56]. The momentum integral of the Boltzmann equation (B1) is

$$\frac{g_{\text{deg}}}{(2\pi)^3} \int \frac{\sqrt{-g} d^3P}{P_0} \frac{df}{d\lambda} = \frac{g_{\text{deg}}}{(2\pi)^3} \int \frac{d^3p}{E} C[f], \quad (\text{B8})$$

where we used the equivalence of the integral measures (B3) and (B7). We aim to show that this equation is equivalent to equation (17). For this purpose it is sufficient to consider the collisionless Boltzmann equation, since the collision terms are already identical. Let f denote the distribution function, and consider

$$\frac{df}{d\lambda} = \frac{dx^\mu}{d\lambda} \frac{\partial f}{\partial x^\mu} + \frac{dP^i}{d\lambda} \frac{\partial f}{\partial P^i} = 0, \quad (\text{B9})$$

that is

$$P^\mu \frac{\partial f}{\partial x^\mu} - \Gamma^i{}_{\mu\nu} P^\mu P^\nu \frac{\partial f}{\partial P^i} = 0. \quad (\text{B10})$$

Integrating both sides of equation (B10) with the integral measure $(\sqrt{-g}^2/P_0) d^3P d^4x$ gives

$$\begin{aligned} & \int \left(P^\mu \frac{\partial f}{\partial x^\mu} - \Gamma^i{}_{\mu\nu} P^\mu P^\nu \frac{\partial f}{\partial P^i} \right) \frac{\sqrt{-g}^2}{P_0} d^3P d^4x \\ &= \int \frac{\partial}{\partial x^\mu} \left(P^\mu f \frac{\sqrt{-g}^2}{P_0} \right) d^3P d^4x \\ & \quad - \int \frac{\partial}{\partial P^i} \left(\Gamma^i{}_{\mu\nu} P^\mu P^\nu f \frac{\sqrt{-g}^2}{P_0} \right) d^3P d^4x = 0. \end{aligned} \quad (\text{B11})$$

The second line of equation (B11) can be rewritten as

$$\begin{aligned} & \int \frac{\partial}{\partial x^\mu} \left(P^\mu f \frac{\sqrt{-g}^2}{P_0} \right) d^3P d^4x \\ &= \int \left[\frac{\partial}{\partial x^\mu} \left(\int P^\mu f \sqrt{-g} \frac{d^3P}{P_0} \right) \right. \\ & \quad \left. + \Gamma^\kappa{}_{\mu\kappa} \int P^\mu f \sqrt{-g} \frac{d^3P}{P_0} \right] \sqrt{-g} d^4x \\ &= \int \left(\int P^\mu f \sqrt{-g} \frac{d^3P}{P_0} \right)_{;\mu} \sqrt{-g} d^4x, \end{aligned} \quad (\text{B12})$$

where we used

$$\begin{aligned} A^\mu{}_{;\mu} &= \frac{\partial A^\mu}{\partial x^\mu} + \Gamma^\mu{}_{\mu\sigma} A^\sigma \\ &= \frac{\partial A^\mu}{\partial x^\mu} + \frac{\partial \ln \sqrt{-g}}{\partial x^\mu} A^\mu = \frac{1}{\sqrt{-g}} \frac{\partial (\sqrt{-g} A^\mu)}{\partial x^\mu}, \end{aligned} \quad (\text{B13})$$

$$= \frac{\partial A^\mu}{\partial x^\mu} + \frac{\partial \ln \sqrt{-g}}{\partial x^\mu} A^\mu = \frac{1}{\sqrt{-g}} \frac{\partial (\sqrt{-g} A^\mu)}{\partial x^\mu}, \quad (\text{B14})$$

which follows from

$$\Gamma^\nu{}_{\mu\nu} = \frac{1}{2} g^{\nu\sigma} \frac{\partial g_{\nu\sigma}}{\partial x^\mu} = \frac{\partial \ln \sqrt{-g}}{\partial x^\mu}. \quad (\text{B15})$$

Also, the left-hand side in the third line of equation (B11) vanishes because the volume integral in momentum space can be rewritten as a surface term at infinity where the distribution function f approaches zero. Thus, equation (B11) can be simplified as

$$\int \left(\int P^\mu f \sqrt{-g} \frac{d^3P}{P_0} \right)_{;\mu} \sqrt{-g} d^4x = 0. \quad (\text{B16})$$

Since this holds for any integral over spacetime, the integrand must vanish. Thus we get

$$\left(\int P^\mu f \sqrt{-g} \frac{d^3P}{P_0} \right)_{;\mu} = 0. \quad (\text{B17})$$

On the other hand, number density current $\mathcal{N}^\mu = nU^\mu$ is defined as

$$\mathcal{N}^\mu \equiv \frac{g_{\text{deg}}}{(2\pi)^3} \int P^\mu f \sqrt{-g} \frac{d^3P}{P_0}, \quad (\text{B18})$$

and hence the momentum integral of the collisionless Boltzmann equation (B9) becomes

$$\mathcal{N}^\mu{}_{;\mu} = 0. \quad (\text{B19})$$

In other words, the left-hand side of equation (B8) can be replaced with $\mathcal{N}^\mu{}_{;\mu}$, which yields the Boltzmann equation in the form of equation (17).

4. Calculation of the covariant derivative of the number density current

In this subsection we calculate equation (18) in detail. In the following we omit the index N_1 in n_{N_1} . By using

equation (19) and formulas in Appendix C,

$$\begin{aligned}
& (nU^\mu)_{;\mu} \\
&= (nU^\mu)_{;\mu} + \Gamma^\mu_{\mu\nu}(nU^\nu) \\
&= (nU^0)_{;0} + \Gamma^0_{0\nu}(nU^\nu) + (nU^i)_{;i} + \Gamma^i_{i\nu}(nU^\nu) \\
&= \left[\frac{n}{a}(1-A) \right]' + \Gamma^0_{00}(nU^0) + \Gamma^0_{0i}(nU^i) \\
&\quad + \left(\frac{n}{a}v^i \right)_{;i} + \Gamma^i_{i0}(nU^0) + \Gamma^i_{ij}(nU^j) \\
&= \frac{n'}{a}(1-A) - \frac{a'}{a^2}n(1-A) - \frac{n}{a}A' \\
&\quad + \left(\frac{a'}{a} + A' \right) \frac{n}{a}(1-A) - \left(A_{;i} - \frac{a'}{a}B_{;i} \right) \frac{n}{a}v^i + \frac{n}{a}v^i_{;i} \\
&\quad + \left[\frac{a'}{a}\delta^i_{;i} + C'\delta^i_{;i} + \left(E^i_{;i} - \frac{1}{3}\delta^i_{;i}\nabla^2 E \right)' \right] \frac{n}{a}(1-A) \\
&\quad + (\text{1st-order}) \times (\text{1st-order}). \tag{B20}
\end{aligned}$$

Dropping the terms of second or higher order in perturbations,

$$\begin{aligned}
& (nU^\mu)_{;\mu} \\
&\simeq \frac{n'}{a}(1-A) - \frac{a'}{a^2}n(1-A) - \frac{n}{a}A' \\
&\quad + \frac{a'}{a}\frac{n}{a}(1-A) + A'\frac{n}{a} + 2\frac{n}{a}v^i_{;i} \\
&\quad + 3\left(\frac{a'}{a} + C' \right) \frac{n}{a} - 3\frac{a'}{a}A\frac{n}{a} \\
&= \frac{n'}{a}(1-A) + \frac{n}{a}v^i_{;i} + 3\frac{a'}{a}\frac{n}{a} + 3C'\frac{n}{a} - 3\frac{a'}{a}A\frac{n}{a} \\
&= (1-A)\left(a^{-1}n' + 3\frac{a'}{a^2}n \right) + \frac{n}{a}(v^i_{;i} + 3C') \\
&= \bar{z}H(1-A)\left(\frac{dn}{d\bar{z}} + \frac{3}{\bar{z}}n \right) + \frac{n}{a}(v^i_{;i} + 3C'), \tag{B21}
\end{aligned}$$

is obtained. Here we used

$$\frac{d}{d\eta} = a\frac{d}{dt} = a\bar{z}H\frac{d}{d\bar{z}}, \tag{B22}$$

that follows from entropy conservation.

5. Calculation of the collision term

In this subsection we calculate equation (20) in detail. The distribution function of right-handed neutrinos, defined with the normalization constant \mathcal{C} , is given by

$$f_{N_1} = \mathcal{C} \exp \left[-\frac{(p_{N_1}^2 + M_1^2)^{1/2} - \mu_{N_1}}{\bar{T} + \delta T} \right]. \tag{B23}$$

By integrating this equation over the entire momentum space, we obtain the particle number density

$$\begin{aligned}
n_{N_1}(\bar{z}) &= \frac{g_{N_1}\mathcal{C}}{2\pi^2} \int_0^\infty dp_{N_1} p_{N_1}^2 \\
&\quad \times \exp \left[-\frac{(p_{N_1}^2 + M_1^2)^{1/2} - \mu_{N_1}}{\bar{T} + \delta T} \right]. \tag{B24}
\end{aligned}$$

Changing the variable to $p_{N_1} = M_1 \sinh \theta$ on the right-hand side, and introducing $z_T(\bar{z}) = \bar{z}/(1 + \delta T)$, the integral reduces to

$$n_{N_1}(\bar{z}) = \frac{g_{N_1}\mathcal{C}}{8\pi^2} M_1^3 \int_0^\infty d\theta (\cosh 3\theta - \cosh \theta) e^{-z_T \cosh \theta}. \tag{B25}$$

Here note that the modified Bessel function of the second kind K_ν is given by the integral

$$K_\nu(z) = \int_0^\infty d\theta \cosh(\nu\theta) e^{-z \cosh \theta}, \tag{B26}$$

from which follows

$$K_{\nu+1}(z) - K_{\nu-1}(z) = \frac{2\nu}{z} K_\nu(z). \tag{B27}$$

Then the normalization constant is determined to be

$$\mathcal{C} = \frac{2\pi^2 z_T}{g_{N_1} M_1^3 K_2(z_T)} n_{N_1}(\bar{z}) e^{-\mu_{N_1}/(\bar{T} + \delta T)}, \tag{B28}$$

and the distribution function of right-handed neutrinos becomes

$$f_{N_1} = \frac{2\pi^2 z_T n_{N_1}(\bar{z})}{g_{N_1} M_1^3 K_2(z_T)} \exp \left[-\frac{(p_{N_1}^2 + M_1^2)^{1/2}}{\bar{T} + \delta T} \right], \tag{B29}$$

which rewrite as $f_{N_1} = \mathcal{C}' n_{N_1}(\bar{z}) e^{-E_{N_1}/(\bar{T} + \delta T)}$. On the other hand, assuming that lepton l and Higgs ϕ are in thermal equilibrium and denoting their distribution functions by f_l^{eq} and f_ϕ^{eq} , respectively, the momentum integral of the collision term in the Boltzmann equation for N_1 is

$$\begin{aligned}
& \frac{g_{N_1}}{(2\pi)^3} \int \frac{d^3 p_{N_1}}{E_{N_1}} \mathcal{C}[f_{N_1}] \\
&= \int d\Pi_{N_1} \int d\Pi_l \int d\Pi_\phi (2\pi)^4 |\mathcal{M}|^2 \delta^4(p_{N_1} - p_l - p_\phi) \\
&\quad \times (f_l^{\text{eq}} f_\phi^{\text{eq}} - f_{N_1}) \\
&= - \int d\Pi_{N_1} \int d\Pi_l \int d\Pi_\phi (2\pi)^4 |\mathcal{M}|^2 \delta^4(p_{N_1} - p_l - p_\phi) \\
&\quad \times \mathcal{C}' \left[n_{N_1}(\bar{z}) e^{-E_{N_1}/(\bar{T} + \delta T)} - n_l^{\text{eq}} n_\phi^{\text{eq}} e^{-(E_l + E_\phi)/(\bar{T} + \delta T)} \right] \\
&\simeq - \int d\Pi_{N_1} \int d\Pi_l \int d\Pi_\phi (2\pi)^4 |\mathcal{M}|^2 \delta^4(p_{N_1} - p_l - p_\phi) \\
&\quad \times \mathcal{C}' e^{-E_{N_1}/(\bar{T} + \delta T)} [n_{N_1}(\bar{z}) - n_{N_1}^{\text{eq}}(z_T)], \tag{B30}
\end{aligned}$$

where we used the energy conservation law $E_{N_1} = E_l + E_\phi$ and detailed balance at high temperatures $n_{N_1}^{\text{eq}} \simeq n_l^{\text{eq}} n_\phi^{\text{eq}}$. Note that the matrix elements for $N_1 \rightarrow l_\alpha \phi$ and $N_1 \rightarrow \bar{l}_\alpha \phi^*$ do not depend on p_{N_1} , p_l , and p_ϕ at the tree level. Let us proceed to perform the integrals over $d\Pi_\phi$, $d\Pi_l$, and $d\Pi_{N_1}$ sequentially. First, for the $d\Pi_\phi$ integral we get

$$\begin{aligned} & \frac{g_{N_1}}{(2\pi)^3} \int \frac{d^3 p_{N_1}}{E_{N_1}} C[f_{N_1}] \\ &= -8\pi^2 |\mathcal{M}|^2 \int \frac{d^3 p_{N_1}}{(2\pi)^3} \frac{g_{N_1}}{2E_{N_1}} \int \frac{d^3 p_l}{(2\pi)^3} \frac{g_l}{2p_l} \frac{g_\phi}{2(E_{N_1} - p_l)} \\ & \times \delta(E_{N_1} - p_l - p_\phi) \mathcal{C}' e^{-E_{N_1}/(\bar{T} + \delta T)} [n_{N_1}(\bar{z}) - n_{N_1}^{\text{eq}}(z_T)]. \end{aligned} \quad (\text{B31})$$

Here we approximated the lepton l and Higgs ϕ to be massless, assuming that their masses are sufficiently smaller than that of the right-handed neutrino N_1 . Thus, performing the integral over $d^3 p_l = 4\pi p_l^2 dp_l$ we get

$$\begin{aligned} & \frac{g_{N_1}}{(2\pi)^3} \int \frac{d^3 p_{N_1}}{E_{N_1}} C[f_{N_1}] \\ &= -|\mathcal{M}|^2 \int \frac{d^3 p_{N_1}}{(2\pi)^3} \frac{g_{N_1}}{2E_{N_1}} \frac{g_l g_\phi (E_{N_1} - p_\phi)}{E_{N_1} - p_l} \\ & \times \mathcal{C}' e^{-E_{N_1}/(\bar{T} + \delta T)} [n_{N_1}(\bar{z}) - n_{N_1}^{\text{eq}}(z_T)]. \end{aligned} \quad (\text{B32})$$

Recalling that l and ϕ are in thermal equilibrium, we take thermal average over these species. Since both l and ϕ are massless we can set $\langle p_l \rangle = \langle p_\phi \rangle$, which yields

$$\begin{aligned} & \left\langle \frac{g_{N_1}}{(2\pi)^3} \int \frac{d^3 p_{N_1}}{E_{N_1}} C[f_{N_1}] \right\rangle \\ &= -g_{N_1} g_l g_\phi |\mathcal{M}|^2 \int \frac{d^3 p_{N_1}}{(2\pi)^3} \\ & \times \frac{\mathcal{C}' e^{-E_{N_1}/(\bar{T} + \delta T)}}{2E_{N_1}} [n_{N_1}(\bar{z}) - n_{N_1}^{\text{eq}}(z_T)]. \end{aligned} \quad (\text{B33})$$

By changing the variable to $p_{N_1} = M_1 \sinh \theta$, equation (B33) becomes

$$\begin{aligned} & \mathcal{C}' \int_0^\infty \frac{4\pi p_{N_1}^2 dp_{N_1}}{2(p_{N_1}^2 + M_1^2)^{1/2}} e^{-(p_{N_1}^2 + M_1^2)^{1/2}/(\bar{T} + \delta T)} \\ &= 2\pi \mathcal{C}' M_1^2 \int_0^\infty d\theta \sinh^2 \theta e^{-z_T \cosh \theta} \\ &= \frac{4\pi^3}{g_{N_1} M_1} \frac{K_1(z_T)}{K_2(z_T)}, \end{aligned} \quad (\text{B34})$$

where we used equations (B26) and (B27). Substituting equation (B34) into equation (B33), we obtain

$$\begin{aligned} & \left\langle \frac{g_{N_1}}{(2\pi)^3} \int \frac{d^3 p_{N_1}}{E_{N_1}} C \right\rangle \\ &= -\frac{4\pi^3 g_l g_\phi |\mathcal{M}|^2}{M_1} \frac{K_1(z_T)}{K_2(z_T)} [n_{N_1}(\bar{z}) - n_{N_1}^{\text{eq}}(z_T)] \\ &\equiv -\Gamma_D(\bar{z} = \infty) \left\langle \frac{1}{\gamma} \right\rangle (z_T) [n_{N_1}(\bar{z}) - n_{N_1}^{\text{eq}}(z_T)]. \end{aligned} \quad (\text{B35})$$

6. Derivation of $N_{N_1}^{\text{eq}}$

In this subsection we discuss several expression of $N_{N_1}^{\text{eq}}(z_T)$ which holds for different ranges of z_T . Approximating with the Boltzmann distribution, the number density $n_{N_1}^{\text{eq}}(z_T)$ can be approximated using the Boltzmann factor as

$$n_{N_1}^{\text{eq}}(z_T) = \mathcal{C}_0 \int \frac{d^3 p_{N_1}}{(2\pi)^3} \exp\left(-\frac{E_{N_1}}{\bar{T} + \delta T}\right), \quad (\text{B36})$$

where \mathcal{C}_0 is a normalization constant. After changing the variable using $E_{N_1} = (p_{N_1}^2 + M_1^2)^{1/2}$ and $t = E_{N_1}/M_1$, integration by parts yields

$$n_{N_1}^{\text{eq}}(z_T) = \mathcal{C}_0 \frac{M_1^3 z_T}{3} \int_1^\infty dt (t^2 - 1)^{3/2} e^{-z_T t}. \quad (\text{B37})$$

By using the integral expression for the modified Bessel function of the second kind

$$K_\nu(z) = \frac{\sqrt{\pi} (z/2)^\nu}{\Gamma(\nu + \frac{1}{2})} \int_1^\infty dt (t^2 - 1)^{\nu - \frac{1}{2}} e^{-zt}, \quad (\text{B38})$$

equation (B37) becomes

$$n_{N_1}^{\text{eq}}(z_T) = \mathcal{C}_0 \frac{M_1^3 z_T}{3} \cdot \frac{3}{z_T^2} K_2(z_T) = \mathcal{C}_0 \frac{M_1^3}{z_T} K_2(z_T). \quad (\text{B39})$$

If the photon number density is normalized $n_\gamma^{\text{eq}}(z_T) \propto (\bar{T} + \delta T)^3$,

$$N_{N_1}^{\text{eq}}(z_T) = \frac{n_{N_1}^{\text{eq}}(z_T)}{n_\gamma^{\text{eq}}(z_T)} = \mathcal{C}'_0 z_T^2 K_2(z_T). \quad (\text{B40})$$

with some normalization constant \mathcal{C}'_0 . For equation (B40) to hold in the relativistic limit $z_T \ll 1$, it must reduce to (6) in this limit. Since

$$K_2(z) \simeq \frac{2}{z} K_1(z) \simeq \frac{2}{z^2}, \quad z \ll 1, \quad (\text{B41})$$

the normalization constant is fixed from

$$\frac{3}{4} = N_{N_1}^{\text{eq}}(z_T \ll 1) \simeq \mathcal{C}'_0 z_T^2 \cdot \frac{2}{z_T^2} = 2\mathcal{C}'_0, \quad (\text{B42})$$

as $\mathcal{C}'_0 = 3/8$. From this and equation (B40), we obtain

$$N_{N_1}^{\text{eq}}(z_T) = \frac{3}{8} z_T^2 K_2(z_T). \quad (\text{B43})$$

7. Derivation of the washout factor W_{ID}

In this subsection we derive the expression for the washout factor W_{ID} . The decay rate of N_1 is given by

$$\Gamma_D(z) = \tilde{\Gamma}_D \left\langle \frac{1}{\gamma} \right\rangle = \tilde{\Gamma}_D \frac{K_1(z_T)}{K_2(z_T)}, \quad (\text{B44})$$

where $\tilde{\Gamma}_D = \Gamma_D(z = \infty)$ from $\lim_{z \rightarrow \infty} K_1(z)/K_2(z) = 1$.

The inverse decay rate Γ_{ID} is related to the decay rate Γ_D through detailed balance

$$\Gamma_{ID}(z) = \Gamma_D(z) \frac{N_{N_1}^{\text{eq}}(z_T)}{N_l^{\text{eq}} N_\phi^{\text{eq}}}. \quad (\text{B45})$$

The equilibrium number densities of heavy neutrinos, lepton doublets, and Higgs doublets are, as already derived,

$$N_{N_1}^{\text{eq}}(z_T) = \frac{3}{8} z_T^2 K_2(z_T), \quad N_l^{\text{eq}} = \frac{3}{4}, \quad N_\phi^{\text{eq}} = 1. \quad (\text{B46})$$

Hence the contribution of inverse decays to the washout term W_{ID} is

$$W_{ID}(z_T) \equiv \frac{1}{2} \frac{\Gamma_{ID}(z_T)}{\bar{z} H(\bar{z})} = \frac{1}{4} z_T^2 K_2(z_T) \frac{\Gamma_D(z_T)}{\bar{z} H(\bar{z})}. \quad (\text{B47})$$

Substituting equation (B44) and $K \equiv \tilde{\Gamma}_D/\bar{z}^2 H(\bar{z})$ into equation (B47), the washout factor is found to be

$$\begin{aligned} W_{ID}(z_T) &= \frac{1}{4} z_T^2 K_2(z_T) \frac{\tilde{\Gamma}_D}{\bar{z} H(\bar{z})} \cdot \frac{K_1(z_T)}{K_2(z_T)} \\ &= \frac{1}{4} K \bar{z} z_T^2 K_1(z_T). \end{aligned} \quad (\text{B48})$$

Appendix C: Perturbative Christoffel symbols

In this appendix we summarize the metric (11)–(13) and its inverse, together with the Christoffel symbols. The metric and its inverse are given by

$$g_{00} = -a^2(1 + 2A), \quad g^{00} = -a^{-2}(1 - 2A), \quad (\text{C1})$$

$$g_{0i} = -a^2 B_{,i}, \quad g^{0i} = -a^{-2} B^{,i}, \quad (\text{C2})$$

$$g_{ij} = a^2 \left[(1 + 2C) \delta_{ij} + 2 \left(E_{,ij} - \frac{1}{3} \delta_{ij} \nabla^2 E \right) \right], \quad (\text{C3})$$

$$g^{ij} = a^{-2} \left[(1 - 2C) \delta^{ij} - 2 \left(E^{,ij} - \frac{1}{3} \delta^{ij} \nabla^2 E \right) \right]. \quad (\text{C4})$$

The Christoffel symbols up to first order in perturbations are given by

$$\Gamma^0_{00} = \frac{a'}{a} + A', \quad (\text{C5})$$

$$\Gamma^0_{0i} = A_{,i} - \frac{a'}{a} B_{,i}, \quad (\text{C6})$$

$$\begin{aligned} \Gamma^0_{ij} &= \frac{a'}{a} \delta_{ij} + \left[-2 \frac{a'}{a} A + \frac{(a^2 C)'}{a^2} \right] \delta_{ij} \\ &\quad + B_{,ij} + \frac{1}{a^2} \left[a^2 \left(E_{,ij} - \frac{1}{3} \delta_{ij} \nabla^2 E \right) \right]', \end{aligned} \quad (\text{C7})$$

$$\Gamma^i_{00} = A^{,i} - \left(B' + \frac{a'}{a} B \right)^{,i}, \quad (\text{C8})$$

$$\Gamma^i_{0j} = \frac{a'}{a} \delta^i_j + C' \delta^i_j + \left(E^{,i}_{,j} - \frac{1}{3} \delta^i_j \nabla^2 E \right)', \quad (\text{C9})$$

$$\begin{aligned} \Gamma^i_{jk} &= (C_{,k} \delta^i_j + C_{,j} \delta^i_k - C^{,i} \delta_{jk}) + \frac{a'}{a} \delta_{jk} B^{,i} \\ &\quad + E^{,i}_{,jk} - \frac{1}{3} \nabla^2 (\delta^i_j E_{,k} + \delta^i_k E_{,j} - \delta_{jk} E^{,i}). \end{aligned} \quad (\text{C10})$$

Appendix D: Calculation of CP asymmetry ε_1

In this appendix we calculate the CP asymmetry ε_1 from the interference between tree and one-loop diagrams in the decay of N_1 .

1. Prerequisites

The relevant Yukawa terms in the Lagrangian are

$$\mathcal{L} \supset -y_{\alpha\beta}^{(e)} (\bar{l}_L)_\alpha \phi (e_R)_\beta - y_{\alpha\beta}^{(\nu)} [(\bar{l}_L)_\alpha \circ \phi^\dagger] N_\beta + \text{h.c.}, \quad (\text{D1})$$

where $\alpha, \beta = 1, 2, 3$ denote the lepton flavor, and repeated indices are implicitly summed over. In addition, the indices L and R represent the left-chiral and right-chiral eigenvectors of the eigenspace (F5) of chirality (F2).

Left-chiral field l_L and Higgs field ϕ form SU(2) doublets as

$$l_L = \begin{pmatrix} \nu_L \\ e_L \end{pmatrix}_{\text{SU}(2)}, \quad \phi = \begin{pmatrix} \phi^+ \\ \phi^0 \end{pmatrix}_{\text{SU}(2)}. \quad (\text{D2})$$

The Dirac conjugate of the former is defined as

$$\bar{l}_L = (\bar{\nu}_L \quad \bar{e}_L)_{\text{SU}(2)}, \quad (\text{D3})$$

where ν_L, ν_R, e_L, e_R are all Weyl fields. The Dirac conjugates for them are defined by promoting to Dirac fields and then projecting them onto the eigenspaces of the chirality γ_5 . To do so we introduce dummy fields ν'_R and e'_R as

$$\nu = \begin{pmatrix} \nu_L \\ \nu'_R \end{pmatrix}_{\text{Dirac}}, \quad e = \begin{pmatrix} e_L \\ e'_R \end{pmatrix}_{\text{Dirac}}, \quad (\text{D4})$$

and then $\bar{\nu}_L$ and \bar{e}_L satisfy

$$\bar{\nu}_L = \overline{P_L \nu} = (P_L \nu)^\dagger \gamma^0 = \nu^\dagger P_L \gamma^0 = \nu^\dagger \gamma^0 P_R, \quad (\text{D5})$$

$$\bar{e}_L = \overline{P_L e} = (P_L e)^\dagger \gamma^0 = e^\dagger P_L \gamma^0 = e^\dagger \gamma^0 P_R, \quad (\text{D6})$$

where P_L and P_R are projection operators of chirality defined in equation (F4). These definitions give

$$l = \begin{pmatrix} \nu \\ e \end{pmatrix}_{\text{SU}(2)} = \begin{pmatrix} \begin{pmatrix} \nu_L \\ \nu'_R \end{pmatrix}_{\text{Dirac}} \\ \begin{pmatrix} e_L \\ e'_R \end{pmatrix}_{\text{Dirac}} \end{pmatrix}_{\text{SU}(2)}$$

$$\Rightarrow l_L = P_L l = \begin{pmatrix} P_L \nu \\ P_L e \end{pmatrix}_{\text{SU}(2)} = \begin{pmatrix} \nu_L \\ e_L \end{pmatrix}_{\text{SU}(2)}. \quad (\text{D7})$$

The product $\bar{l}_L \circ \phi^\dagger$ is defined so that it is invariant under SU(2) [Note that $i\sigma^2 = \begin{pmatrix} 0 & 1 \\ -1 & 0 \end{pmatrix}$]:

$$\begin{aligned} \bar{l}_L \circ \phi^\dagger &= (\bar{\nu}_L \ \bar{e}_L)_{\text{SU}(2)} \circ \begin{pmatrix} (\phi^+)^\dagger \\ (\phi^0)^\dagger \end{pmatrix}_{\text{SU}(2)} \\ &= (\bar{\nu}_L \ \bar{e}_L)_{\text{SU}(2)} \begin{pmatrix} 0 & 1 \\ -1 & 0 \end{pmatrix} \begin{pmatrix} (\phi^+)^\dagger \\ (\phi^0)^\dagger \end{pmatrix}_{\text{SU}(2)} \\ &= \bar{\nu}_L (\phi^0)^\dagger - \bar{e}_L (\phi^+)^\dagger, \end{aligned} \quad (\text{D8})$$

which can be rewritten as

$$\bar{l}_L \circ \phi^\dagger = \overline{P_L l} \circ \phi^\dagger = (\bar{l} P_R) \circ \phi^\dagger = (\bar{l} \circ \phi^\dagger) P_R. \quad (\text{D9})$$

The conjugate of the above gives $\phi \circ l_L$:

$$\begin{aligned} \phi \circ l_L &= \begin{pmatrix} \phi^+ & \phi^0 \end{pmatrix}_{\text{SU}(2)} \circ \begin{pmatrix} \nu_L \\ e_L \end{pmatrix}_{\text{SU}(2)} \\ &= \begin{pmatrix} \phi^+ & \phi^0 \end{pmatrix}_{\text{SU}(2)} \begin{pmatrix} 0 & 1 \\ -1 & 0 \end{pmatrix} \begin{pmatrix} \nu_L \\ e_L \end{pmatrix}_{\text{SU}(2)} \\ &= \nu_L \phi^0 - e_L \phi^+, \end{aligned} \quad (\text{D10})$$

which can be rewritten as

$$\phi \circ l_L = P_L (\phi \circ l). \quad (\text{D11})$$

Note that the sign of the operation \circ changes depending on whether the fields are SU(2) fundamental or SU(2) anti-fundamental.

The Majorana field N is the Majorana representation of the right-chiral Weyl field ν_R given by

$$N = \begin{pmatrix} (\nu_R)^c \\ \nu_R \end{pmatrix}_{\text{Dirac}}, \quad (\text{D12})$$

where the charge conjugation operator c is defined as

$$\begin{aligned} (\text{left-chiral})^c &= i\sigma^2 (\text{left-chiral})^\dagger, \\ (\text{right-chiral})^c &= -i\sigma^2 (\text{right-chiral})^\dagger, \end{aligned} \quad (\text{D13})$$

thereby $(\nu_R)^c = -i\sigma^2 \nu_R^\dagger$. Thus the relevant Yukawa couplings become

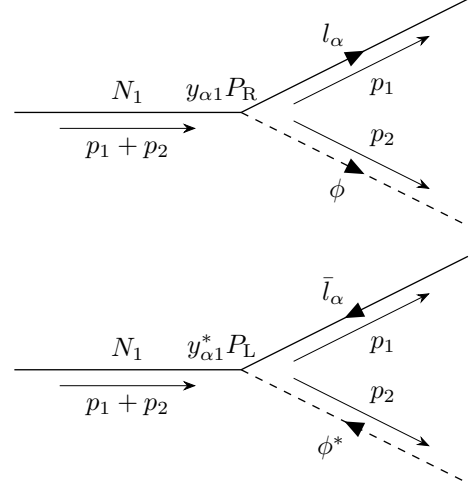
$$\begin{aligned} \mathcal{L}_{\text{int}} &= -y_{\alpha\beta}^{(\nu)} [(\bar{l}_L)_\alpha \circ \phi^\dagger] N_\beta + \text{h.c.} \\ &= -y_{\alpha\beta}^{(\nu)} (\bar{l}_\alpha \circ \phi^\dagger) P_R N_\beta - y_{\alpha\beta}^{(\nu)*} \bar{N}_\beta P_L (\phi \circ l_\alpha). \end{aligned} \quad (\text{D14})$$

Henceforth, we denote $y_{\alpha\beta}^{(\nu)}$ by $y_{\alpha\beta}$.

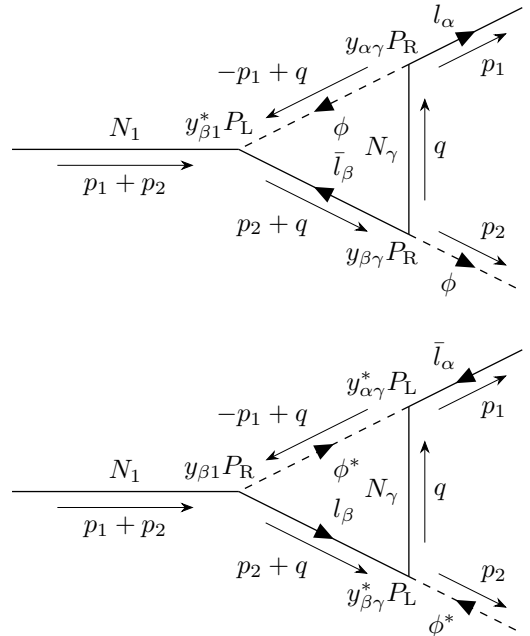
2. Feynman diagrams

We list the Feynman diagrams that appear in the one-loop calculation of ε_1 . For the Feynman rules for Majorana fermions, refer to Refs. [57, 58].

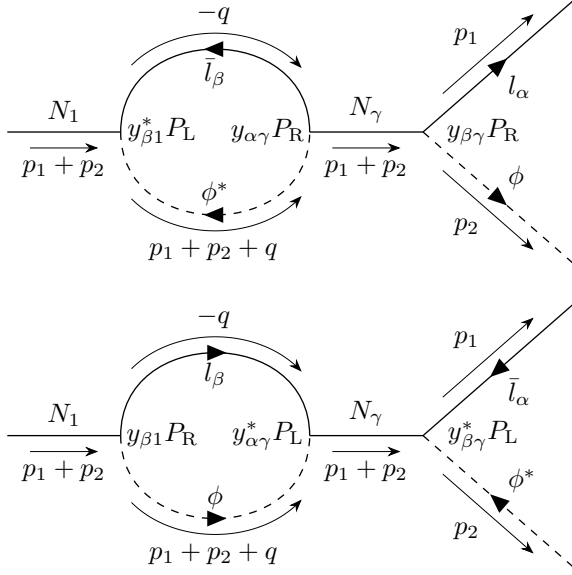
a. Tree diagrams



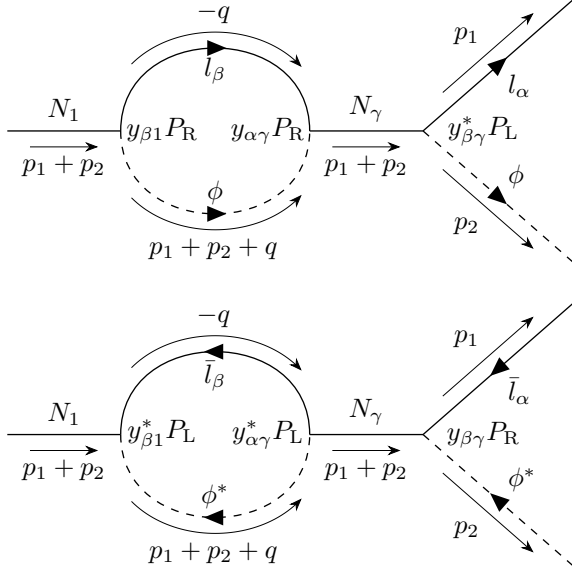
b. Vertex diagrams



c. Wavefunction diagrams I



d. Wavefunction diagrams II



3. Calculation of tree diagrams

In this subsection we calculate the tree diagrams. Hereafter we assume that the masses of the leptons and the Higgs boson are negligible compared to the mass of the heavy neutrino M_1 . We often use

$$p_1^2 = p_2^2 = 0, \quad p_1 \cdot p_2 = \frac{M_1^2}{2}, \quad (\text{D15})$$

for the momenta of the lepton p_1 and the Higgs boson p_2 . Here the second equation is derived from $(p_1 + p_2)^2 = M_1^2$.

First we consider $N_1 \rightarrow l_\alpha \phi$. Let s and t be the spins of the initial and final states of N_1 and l_α , respectively. The Lagrangian in equation (D14) can be written as

$$\mathcal{L}_{\text{int}} \supset -y_{\alpha\beta} [\bar{\nu}_\alpha(\phi^0)^\dagger - \bar{e}_\alpha(\phi^+)^\dagger] P_R N_\beta. \quad (\text{D16})$$

Thus there are two possibilities for the final state: $\nu_\alpha \phi^0$ and $e_\alpha \phi^+$, originating from the SU(2) doublet. Here the matrix element $i\mathcal{M}_{N_1 \rightarrow l_\alpha \phi}^{(s,t)}$ is defined for each channel, and hence the result obtained below must be multiplied by a factor of two when calculating the total decay rate. The total matrix element is the sum of the tree and the one-loop:

$$i\mathcal{M}_{N_1 \rightarrow l_\alpha \phi}^{(\text{tree}+1\text{-loop})(s,t)} = i\mathcal{M}_{N_1 \rightarrow l_\alpha \phi}^{(\text{tree})(s,t)} + i\mathcal{M}_{N_1 \rightarrow l_\alpha \phi}^{(1\text{-loop})(s,t)}. \quad (\text{D17})$$

The squared magnitude of the matrix element at the tree level is obtained by taking the sum over spins s and t and then averaging over the spin s of the initial state

$$\begin{aligned} \left| \overline{i\mathcal{M}}_{N_1 \rightarrow l_\alpha \phi}^{(\text{tree})} \right|^2 &\equiv \frac{1}{2} \sum_{s,t} \left| i\mathcal{M}_{N_1 \rightarrow l_\alpha \phi}^{(\text{tree})(s,t)} \right|^2 \\ &= \frac{1}{2} \sum_{s,t} \left| \bar{u}_{l_\alpha}^t(p_1) (-iy_{\alpha 1} P_R) u_{N_1}^s(p_1 + p_2) \right|^2 \\ &= \frac{1}{2} |y_{\alpha 1}|^2 \text{tr}[(\not{p}_1 + \not{p}_2 + M_1) P_L \not{p}_1 P_R] \\ &= |y_{\alpha 1}|^2 (p_1 \cdot p_2) = \frac{1}{2} |y_{\alpha 1}|^2 M_1^2, \end{aligned} \quad (\text{D18})$$

where we used the spin sum formula (F23), the trace formulas (F10), (F11), (F14), and (F3), as well as the approximation in equation (D15).

Next, for $N_1 \rightarrow \bar{l}_\alpha \phi^*$, a similar calculation yields

$$\begin{aligned} \left| \overline{i\mathcal{M}}_{N_1 \rightarrow \bar{l}_\alpha \phi^*}^{(\text{tree})} \right|^2 &\equiv \frac{1}{2} \sum_{s,t} \left| i\mathcal{M}_{N_1 \rightarrow \bar{l}_\alpha \phi^*}^{(\text{tree})(s,t)} \right|^2 \\ &= \frac{1}{2} \sum_{s,t} \left| \bar{v}_{l_\alpha}^t(p_1) (-iy_{\alpha 1}^* P_L) u_{N_1}^s(p_1 + p_2) \right|^2 \\ &= \frac{1}{2} |y_{\alpha 1}|^2 \text{tr}[(\not{p}_1 + \not{p}_2 - M_1) P_R \not{p}_1 P_L] \\ &= |y_{\alpha 1}|^2 (p_1 \cdot p_2) = \frac{1}{2} |y_{\alpha 1}|^2 M_1^2. \end{aligned} \quad (\text{D19})$$

4. Calculation of vertex diagrams

In this subsection we calculate vertex diagrams and the resulting interference with the tree-level diagrams. We first consider $N_1 \rightarrow l_\alpha \phi$. The combined contribution

of the tree and one-loop diagrams is

$$\begin{aligned} \left| \overline{i\mathcal{M}}_{N_1 \rightarrow l_\alpha \phi}^{(\text{tree}+1\text{-loop})} \right|^2 &\equiv \frac{1}{2} \sum_{s,t} \left| i\mathcal{M}_{N_1 \rightarrow l_\alpha \phi}^{(\text{tree}+1\text{-loop})(s,t)} \right|^2 \\ &\simeq \frac{1}{2} \sum_{s,t} \left| i\mathcal{M}_{N_1 \rightarrow l_\alpha \phi}^{(\text{tree})(s,t)} \right|^2 \\ &\quad + \frac{1}{2} \sum_{s,t} \left[\left(i\mathcal{M}_{N_1 \rightarrow l_\alpha \phi}^{(\text{tree})(s,t)} \right)^* \left(i\mathcal{M}_{N_1 \rightarrow l_\alpha \phi}^{(1\text{-loop})(s,t)} \right) + \text{c.c.} \right]. \end{aligned} \quad (\text{D20})$$

The interference part is

$$\begin{aligned} I_{\text{vertex}} &\equiv \frac{1}{2} \sum_{s,t} \left(i\mathcal{M}_{N_1 \rightarrow l_\alpha \phi}^{(\text{tree})(s,t)} \right)^* \left(i\mathcal{M}_{N_1 \rightarrow l_\alpha \phi}^{(1\text{-loop})(s,t)} \right) \\ &= iy_{\alpha 1}^* y_{\beta 1}^* y_{\alpha \gamma} y_{\beta \gamma} \\ &\quad \times \int \frac{d^4 q}{(2\pi)^4} \frac{-\frac{1}{2} M_1^3 M_\gamma - M_1 M_\gamma (p_1 \cdot q)}{(q^2 - M_\gamma^2)(-p_2 - q)^2(-p_1 + q)^2} \\ &\equiv y_{\alpha 1}^* y_{\beta 1}^* y_{\alpha \gamma} y_{\beta \gamma} D_{\text{vertex}}, \end{aligned} \quad (\text{D21})$$

where we used equation (F6), the spin sum formula (F23), and the trace formulas (F10), (F11), (F13). Furthermore, performing the q -integration using Feynman parametrization (F26) and the dimensional regularization formulas (F27) and (F28), we get

$$\begin{aligned} D_{\text{vertex}} &= \frac{1}{2} \int \frac{d^4 q}{i(2\pi)^4} \\ &\quad \times \frac{M_1^3 M_\gamma + 2M_1 M_\gamma (p_1 \cdot q)}{(q^2 - M_\gamma^2 + i\epsilon)(-p_2 - q + i\epsilon)^2(-p_1 + q + i\epsilon)^2} \\ &= \frac{M_1^2}{32\pi^2} \int_0^1 dx \int_0^{1-x} dy \frac{M_1 M_\gamma (1-y)}{M_\gamma^2 (1-x-y) - M_1^2 xy - i\epsilon}, \end{aligned} \quad (\text{D22})$$

where $-i\epsilon$ in the denominator comes from the $i\epsilon$ prescription.

We define $m \equiv M_1/M_\gamma$ and perform the integration over y in equation (D22). Considering the complex y -plane, there exists a pole at $y = (1-x)/(1+m^2x) \equiv a$ within the range $0 \leq y \leq 1-x$ on the real axis, which we avoid by taking an upper semicircle. We divide the integration range of y into three intervals $[0, a - \epsilon']$, $[a - \epsilon', a + \epsilon']$, and $[a + \epsilon', 1]$. In the middle interval $[a - \epsilon', a +$

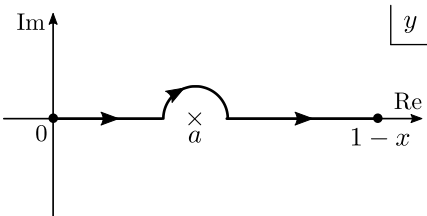


FIG. 11. Contour of D_{vertex} .

$\epsilon']$, we perform the variable transformation $y = a + \epsilon' e^{i\theta}$ (where $\epsilon' > 0$ is a small quantity and $0 \leq \theta \leq \pi$). The imaginary part of D_{vertex} is evaluated as

$$\begin{aligned} i \text{Im}(D_{\text{vertex}}) &= \frac{M_1^2}{32\pi^2} \int_0^1 dx \int_{a-\epsilon'}^{a+\epsilon'} dy \frac{m(1-y)}{1-x-y-m^2xy-i\epsilon} \\ &= -\frac{M_1^2}{32\pi^2} \int_0^1 dx \frac{m}{1+m^2x} \int_{a-\epsilon'}^{a+\epsilon'} dy \frac{y-1}{y-\frac{1-x}{1+m^2x}+i\epsilon} \\ &= -\frac{M_1^2}{32\pi^2} \int_0^1 dx \frac{m}{1+m^2x} \int_\pi^0 i\epsilon' e^{i\theta} d\theta \frac{a-1+\mathcal{O}(\epsilon')}{\epsilon' e^{i\theta}} \\ &\xrightarrow{\epsilon' \downarrow 0} -\frac{M_1^2}{32\pi^2} \int_0^1 dx (-i\pi) \frac{m}{1+m^2x} \left(\frac{1-x}{1+m^2x} - 1 \right), \end{aligned} \quad (\text{D23})$$

where the $+i\epsilon$ in the denominator specifies that the integration contour lies in the upper half-plane.

Upon performing the x -integration, we find

$$\text{Im}(D_{\text{vertex}}) = \frac{M_1^2}{32\pi} \left\{ \frac{1}{m} \left[1 - \left(1 + \frac{1}{m^2} \right) \ln(1+m^2) \right] \right\}. \quad (\text{D24})$$

Thus equation (D21) becomes

$$I_{\text{vertex}} = iy_{\alpha 1}^* y_{\beta 1}^* y_{\alpha \gamma} y_{\beta \gamma} \text{Im}(D_{\text{vertex}}). \quad (\text{D25})$$

We next consider $N_1 \rightarrow \bar{l}_\alpha \phi^*$. Similar calculation as above gives

$$\begin{aligned} I'_{\text{vertex}} &\equiv \frac{1}{2} \sum_{s,t} \left(i\mathcal{M}_{N_1 \rightarrow \bar{l}_\alpha \phi^*}^{(\text{tree})(s,t)} \right)^* \left(i\mathcal{M}_{N_1 \rightarrow \bar{l}_\alpha \phi^*}^{(1\text{-loop})(s,t)} \right) \\ &= \dots \\ &= iy_{\alpha 1} y_{\beta 1} y_{\alpha \gamma}^* y_{\beta \gamma}^* \frac{M_1^2}{32\pi} \left\{ \frac{1}{m} \left[1 - \left(1 + \frac{1}{m^2} \right) \ln(1+m^2) \right] \right\}. \end{aligned} \quad (\text{D26})$$

Regarding the external lines, while the anti-lepton part changed from $u_{l_\alpha}^t$ to $v_{l_\alpha}^t$, the N_1 part remained as $u_{N_1}^s$. This is due to the Majorana nature of N_1 .

Combining above results, the CP asymmetry $(\varepsilon_1)_{\text{vertex}}$ is given by

$$\begin{aligned} (\varepsilon_1)_{\text{vertex}} &= \frac{\sum_\alpha \left(\left| \overline{i\mathcal{M}}_{N_1 \rightarrow l_\alpha \phi}^{(\text{tree}+1\text{-loop})} \right|^2 - \left| \overline{i\mathcal{M}}_{N_1 \rightarrow \bar{l}_\alpha \phi^*}^{(\text{tree}+1\text{-loop})} \right|^2 \right)}{\sum_\alpha \left(\left| \overline{i\mathcal{M}}_{N_1 \rightarrow l_\alpha \phi}^{(\text{tree})} \right|^2 + \left| \overline{i\mathcal{M}}_{N_1 \rightarrow \bar{l}_\alpha \phi^*}^{(\text{tree})} \right|^2 \right)} \\ &= \frac{\text{Im}(y_{\alpha 1} y_{\beta 1} y_{\alpha \gamma}^* y_{\beta \gamma}^*)}{8\pi \sum_\alpha |y_{\alpha 1}|^2} F(m), \quad m \equiv \frac{M_1}{M_\gamma}, \\ F(m) &\equiv \frac{1}{m} \left[1 - \left(1 + \frac{1}{m^2} \right) \ln(1+m^2) \right]. \end{aligned} \quad (\text{D27})$$

As seen from this expression, in order for ε_1 to be non-zero, D_{vertex} must have an imaginary part.

5. Calculation of wavefunction diagrams

Regarding the wavefunction diagrams, there appears two types of contributions: wavefunction I and wavefunction II. However, only the former contributes to the CP asymmetry (this will be verified later). Additionally, be mindful of the factor two which appears below. This arises when two different particle species belonging to the SU(2) group appear in the loop. For example, when fix the decay channel to $N_\alpha \rightarrow \nu_\alpha \phi^0$, the particles appearing in the triangular loop in the vertex diagrams are fixed to ϕ^0 and ν_β , since the vertex is connected to the final state. On the other hand, in the wavefunction diagrams, there is no constraint on the particles entering the loop from the final state, and hence both $\nu_\alpha \phi^0$ and $e_\alpha \phi^+$ contribute.

The interference term of the wavefunction diagram I is

$$\begin{aligned} I_{\text{wave}}^{(1)} &= \frac{1}{2} \sum_{s,t} \left(i\mathcal{M}_{N_1 \rightarrow l_\alpha \phi}^{(\text{tree})(s,t)} \right)^* \left(i\mathcal{M}_{N_1 \rightarrow l_\alpha \phi}^{(1\text{-loop})(s,t)} \right) \\ &= iy_{\alpha 1}^* y_{\beta 1}^* y_{\alpha \gamma} y_{\beta \gamma} \frac{2M_1 M_\gamma}{M_1^2 - M_\gamma^2} \int \frac{d^4 q}{(2\pi)^4} \frac{p_1 \cdot q}{q^2(p_1 + p_2 + q)^2} \\ &\equiv y_{\alpha 1}^* y_{\beta 1}^* y_{\alpha \gamma} y_{\beta \gamma} D_{\text{wave}}^{(1)}, \end{aligned} \quad (\text{D28})$$

where we used (F6), the spin sum formula (F23), and the trace formulas (F10), (F11) and (F14). Furthermore, applying Feynman parametrization (F25) and the dimensional regularization formula (F28), we perform the q -integration and extract the imaginary part, obtaining

$$\begin{aligned} D_{\text{wave}}^{(1)} &= -\frac{2M_1 M_\gamma}{M_1^2 - M_\gamma^2} \int \frac{d^4 q}{i(2\pi)^4} \frac{p_1 \cdot q}{q^2(q + p_1 + p_2)^2} \\ &= -\frac{1}{16\pi^2} \frac{M_1^3 M_\gamma}{M_1^2 - M_\gamma^2} \int_0^1 dx x \log[-M_1^2 x(1-x) - i\epsilon], \end{aligned} \quad (\text{D29})$$

i.e.,

$$\text{Im}(D_{\text{wave}}^{(1)}) = \frac{1}{32\pi} \frac{M_1^3 M_\gamma}{M_1^2 - M_\gamma^2}. \quad (\text{D30})$$

Here note that $\log[-M_1^2 x(1-x) - i\epsilon]$ is specified with the integration contour lying in the lower half-plane, thus yielding $-i\pi$ instead of $+i\pi$. From this and equation (D29), we obtain

$$I_{\text{wave}}^{(1)} = iy_{\alpha 1}^* y_{\beta 1}^* y_{\alpha \gamma} y_{\beta \gamma} \frac{M_1^2}{32\pi} \frac{m}{m^2 - 1}, \quad m \equiv \frac{M_1}{M_\gamma}. \quad (\text{D31})$$

The interference term of the wavefunction diagram II

is

$$\begin{aligned} I_{\text{wave}}^{(2)} &= \frac{1}{2} \sum_{s,t} \left(i\mathcal{M}_{N_1 \rightarrow l_\alpha \phi}^{(\text{tree})(s,t)} \right)^* \left(i\mathcal{M}_{N_1 \rightarrow l_\alpha \phi}^{(1\text{-loop})(s,t)} \right) \\ &= iy_{\alpha 1}^* y_{\beta 1} y_{\alpha \gamma} y_{\beta \gamma}^* \frac{2M_1^2}{M_1^2 - M_\gamma^2} \int \frac{d^4 q}{(2\pi)^4} \frac{p_2 \cdot q}{q^2(p_1 + p_2 + q)^2}, \end{aligned} \quad (\text{D32})$$

where we have taken into account equation (F6), the spin sum formula (F23) and the trace formulas (F12) and (F15). Applying Feynman parametrization (F25) and the dimensional regularization formula (F28), we perform the q -integration in a similar way to those in equation (D31), obtaining

$$I_{\text{wave}}^{(2)} = iy_{\alpha 1}^* y_{\beta 1} y_{\alpha \gamma} y_{\beta \gamma}^* \frac{M_1^2}{32\pi} \frac{m^2}{m^2 - 1}, \quad m \equiv \frac{M_1}{M_\gamma}. \quad (\text{D33})$$

By summing equations (D31) and (D33), similarly to equation (D27), we find

$$\begin{aligned} (\varepsilon_1)_{\text{wave}} &= \frac{\sum_\alpha \left(\left| i\overline{\mathcal{M}}_{N_1 \rightarrow l_\alpha \phi}^{(\text{tree}+1\text{-loop})} \right|^2 - \left| i\overline{\mathcal{M}}_{N_1 \rightarrow \bar{l}_\alpha \phi^*}^{(\text{tree}+1\text{-loop})} \right|^2 \right)}{\sum_\alpha \left(\left| i\overline{\mathcal{M}}_{N_1 \rightarrow l_\alpha \phi}^{(\text{tree})} \right|^2 + \left| i\overline{\mathcal{M}}_{N_1 \rightarrow \bar{l}_\alpha \phi^*}^{(\text{tree})} \right|^2 \right)} \\ &= \frac{\text{Im}(y_{\alpha 1} y_{\beta 1} y_{\alpha \gamma}^* y_{\beta \gamma}^*)}{8\pi \sum_\alpha |y_{\alpha 1}|^2} \cdot \frac{m}{m^2 - 1} \\ &\quad + \frac{\text{Im}(y_{\alpha 1} y_{\beta 1}^* y_{\alpha \gamma}^* y_{\beta \gamma})}{8\pi \sum_\alpha |y_{\alpha 1}|^2} \cdot \frac{m^2}{m^2 - 1}. \end{aligned} \quad (\text{D34})$$

Here note that

$$\begin{aligned} \text{Im}(y_{\alpha 1} y_{\beta 1}^* y_{\alpha \gamma}^* y_{\beta \gamma}) &= \text{Im} \left[\sum_\alpha (y_{\alpha 1} y_{\alpha \gamma}^*) \sum_\beta (y_{\beta 1}^* y_{\beta \gamma}) \right] \\ &= \text{Im} \left(\left| \sum_\alpha y_{\alpha 1} y_{\alpha \gamma}^* \right|^2 \right) = 0, \end{aligned} \quad (\text{D35})$$

from which follows that the contribution from wavefunction diagram II is zero. Thus we find

$$(\varepsilon_1)_{\text{wave}} = \frac{\text{Im}(y_{\alpha 1} y_{\beta 1} y_{\alpha \gamma}^* y_{\beta \gamma}^*)}{8\pi \sum_\alpha |y_{\alpha 1}|^2} \cdot \frac{m}{m^2 - 1}, \quad m \equiv \frac{M_1}{M_\gamma}. \quad (\text{D36})$$

6. Final result and approximate expression

By combining equations (D27) and (D36), the expression for the CP asymmetry is obtained as

$$\begin{aligned} \varepsilon_1 &= \frac{\text{Im}(y_{\alpha 1} y_{\beta 1} y_{\alpha \gamma}^* y_{\beta \gamma}^*)}{8\pi \sum_\alpha |y_{\alpha 1}|^2} \\ &\quad \times \frac{1}{m} \left[1 + \frac{m^2}{m^2 - 1} - \left(1 + \frac{1}{m^2} \right) \ln(1 + m^2) \right]. \end{aligned} \quad (\text{D37})$$

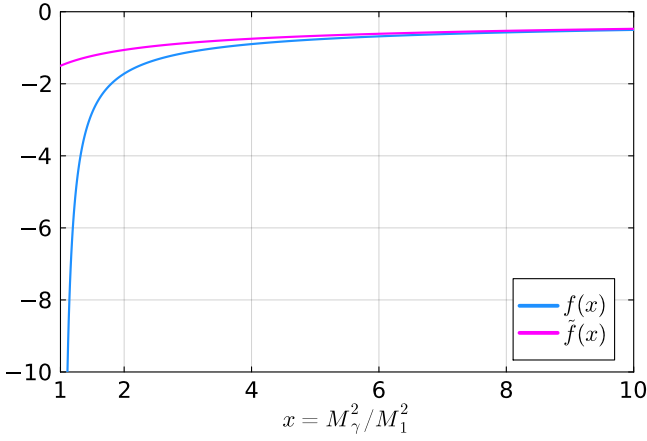


FIG. 12. Functions $f(x)$ (blue) and $\tilde{f}(x) \equiv -3/(2\sqrt{x})$ (magenta).

At this point we switch to $x \equiv M_\gamma^2/M_1^2$ in place of $m \equiv M_1/M_\gamma$ to match the literature

$$\varepsilon_1 = \frac{\text{Im}(y_{\alpha 1} y_{\beta 1} y_{\alpha \gamma}^* y_{\beta \gamma}^*)}{8\pi \sum_\alpha |y_{\alpha 1}|^2} f(x), \quad x \equiv \frac{M_\gamma^2}{M_1^2},$$

$$f(x) \equiv \sqrt{x} \left[1 + \frac{1}{1-x} - (1+x) \ln \left(1 + \frac{1}{x} \right) \right]. \quad (\text{D38})$$

Note that $\text{Im}(y_{\alpha 1} y_{\beta 1} y_{\alpha \gamma}^* y_{\beta \gamma}^*) = 0$ and hence $\varepsilon_1 = 0$ for $\gamma = 1$. Thus the contributions from the second and third generations are necessary to generate nonzero ε_1 .

When the magnitude of the CP asymmetry ε_1 is much smaller than one, $x = M_\gamma^2/M_1^2$ is expected to be much larger than unity. In this case, we perform a Taylor expansion of $f(x)$ for $1/x \ll 1$:

$$f(x) = - \left[\frac{3}{2\sqrt{x}} + \frac{5}{6x^{3/2}} + \mathcal{O}\left(\frac{1}{x^{5/2}}\right) \right], \quad (\text{D39})$$

from which we define \tilde{f} taking the leading term

$$\tilde{f}(x) \equiv -\frac{3}{2\sqrt{x}}. \quad (\text{D40})$$

The plots for $f(x)$ and $\tilde{f}(x)$ are shown in Figure 12. When approximating $f(x)$ with $\tilde{f}(x)$, the CP asymmetry (D38) is approximated as

$$\varepsilon_1 \simeq -\frac{3M_1}{16\pi \sum_\alpha |y_{\alpha 1}|^2} \text{Im} \left(y_{\alpha 1} y_{\alpha \gamma}^* \frac{1}{M_\gamma} y_{\beta 1} y_{\beta \gamma}^* \right). \quad (\text{D41})$$

Appendix E: Derivation of the maximal CP asymmetry $|\varepsilon_1|^{\max}$

From the Lagrangian (2), the neutrino masses are given by [59]

$$\mathcal{L}_m = -\frac{M_{\alpha\beta}}{2} \bar{N}_\alpha^c N_\beta - y_{\alpha\beta} \phi^* \bar{l}_\alpha \bar{N}_\beta + \text{h.c.}, \quad (\text{E1})$$

where M is the heavy neutrino mass matrix. Here $(m_D)_{\alpha\beta} = y_{\alpha\beta} v$ from the Higgs mechanism, where m_D is the Dirac mass matrix, $y_{\alpha\beta}$ is the Yukawa coupling, and $v = \langle \phi \rangle$ is the VEV of the Higgs field ϕ . We adopt the mass eigenstate basis for the heavy neutrinos, in which M is diagonal with real positive eigenvalues $M_1 \leq M_2 \leq M_3$.

Through the seesaw mechanism, the light neutrino mass matrix m_ν can be expressed in terms of m_D and the inverse of M ,

$$m_\nu = -m_D \frac{1}{M} m_D^\top, \quad (\text{E2})$$

where higher order terms in $1/M$ are neglected. m_ν can be diagonalized by a unitary matrix $U^{(\nu)}$

$$U^{(\nu)\dagger} m_\nu U^{(\nu)*} = - \begin{pmatrix} m_1 & 0 & 0 \\ 0 & m_2 & 0 \\ 0 & 0 & m_3 \end{pmatrix} \equiv -D_m, \quad (\text{E3})$$

with real positive eigenvalues $m_1 \leq m_2 \leq m_3$. Substituting equation (E2) into equation (E3), we get

$$U^{(\nu)\dagger} (-m_D M^{-1} m_D^\top) U^{(\nu)*} = -U^{(\nu)\dagger} (y v) D_M^{-1} (y v)^\top U^{(\nu)*} = -v^2 U^{(\nu)\dagger} y D_M^{-1} y^\top U^{(\nu)*} = -D_m, \quad (\text{E4})$$

where D_M is the diagonalized heavy mass matrix M . Equation (E4) means that

$$\Omega \equiv v D_m^{-1/2} U^{(\nu)\dagger} y D_M^{-1/2} \quad (\text{E5})$$

is an orthogonal matrix $\Omega \Omega^\top = \mathbf{1}$. This implies that $\text{Im}(\Omega^\top \Omega)_{11} = 0$, which yields

$$\begin{aligned} 0 &= \text{Im}(\Omega^\top \Omega)_{11} \\ &= \text{Im}(v D_M^{-1/2} y^\top U^{(\nu)*} D_m^{-1/2} \cdot v D_m^{-1/2} U^{(\nu)\dagger} y D_M^{-1/2})_{11} \\ &= v^2 \frac{1}{M_1} \text{Im}(D_m^{-1} y^\top U^{(\nu)*} \cdot U^{(\nu)\dagger} y)_{11} \\ &= v^2 \frac{1}{M_1} \sum_{\alpha=1,2,3} \frac{1}{m_\alpha} \text{Im}(U^{(\nu)\dagger} y)_{\alpha 1}^2, \end{aligned} \quad (\text{E6})$$

that is,

$$\frac{1}{m_1} \text{Im}(U^{(\nu)\dagger} y)_{11}^2 = - \sum_{\alpha \neq 1} \frac{1}{m_\alpha} \text{Im}(U^{(\nu)\dagger} y)_{\alpha 1}^2. \quad (\text{E7})$$

On the other hand, the CP asymmetry ε_1 is obtained from equation (D41)

$$\varepsilon_1 \simeq -\frac{3}{16\pi} \frac{M_1}{(y^\dagger y)_{11}} \text{Im} \left(y^\dagger y \frac{1}{M} y^\top y^* \right)_{11}, \quad (\text{E8})$$

where M is the heavy neutrino mass matrix. Substituting equation (E3) and equation (E7) into (E8), and expressing it in terms of

$$\tilde{y} = U^{(\nu)\dagger} y \quad (\text{E9})$$

instead of y , we obtain

$$\begin{aligned} \text{Im}\left(\tilde{y}^\dagger \tilde{y} \frac{1}{M} \tilde{y}^\dagger \tilde{y}^*\right)_{11} &= -\frac{1}{v^2} \text{Im}\left(\tilde{y}^\dagger U^{(\nu)\dagger} m_\nu U^{(\nu)*} \tilde{y}^*\right)_{11} \\ &= -\frac{m_1}{v^2} \text{Im}(\tilde{y}_{11}^2) - \sum_{\alpha \neq 1} \frac{m_\alpha}{v^2} \text{Im}(\tilde{y}_{\alpha 1}^2) \\ &= -\frac{1}{v^2} \sum_{\alpha \neq 1} \frac{\Delta m_{\alpha 1}^2}{m_\alpha} \text{Im}(\tilde{y}_{\alpha 1}^2), \end{aligned} \quad (\text{E10})$$

that translates into

$$\varepsilon_1 = \frac{3}{16\pi} \frac{M_1}{v^2} \sum_{\alpha \neq 1} \frac{\Delta m_{\alpha 1}^2}{m_\alpha} \frac{\text{Im}(\tilde{y}_{\alpha 1}^2)}{(\tilde{y}^\dagger \tilde{y})_{11}}, \quad (\text{E11})$$

where $\Delta m_{\alpha 1}^2 \equiv m_\alpha^2 - m_1^2$.

Now, consider the normalized Yukawa couplings [46]

$$z_\alpha = \frac{\tilde{y}_{\alpha 1}^2}{(\tilde{y}^\dagger \tilde{y})_{11}} = X_\alpha + iY_\alpha, \quad (\text{E12})$$

which follow

$$0 \leq |z_\alpha| \leq 1, \quad \sum_\alpha |z_\alpha| = 1. \quad (\text{E13})$$

From the orthogonality condition $(\Omega^\dagger \Omega)_{11} = 1$, the additional constraint is given by

$$\sum_\alpha \frac{\tilde{m}_1}{m_\alpha} z_\alpha = 1, \quad (\text{E14})$$

where \tilde{m}_1 is the effective neutrino mass (37). From equation (E11), the CP asymmetry reads in the new variables

$$\varepsilon_1 = \frac{3}{16\pi} \frac{M_1}{v^2} \left(\frac{\Delta m_{21}^2}{m_2} Y_2 + \frac{\Delta m_{31}^2}{m_3} Y_3 \right). \quad (\text{E15})$$

Since $m_3 > m_2$,

$$\begin{aligned} \frac{\Delta m_{31}^2}{m_3} - \frac{\Delta m_{21}^2}{m_2} &= \frac{m_3^2 - m_1^2}{m_3} - \frac{m_2^2 - m_1^2}{m_2} \\ &= \frac{(m_3 - m_2)(m_1^2 + m_2 m_3)}{m_2 m_3} > 0 \\ \Rightarrow \frac{\Delta m_{31}^2}{m_3} &> \frac{\Delta m_{21}^2}{m_2}. \end{aligned} \quad (\text{E16})$$

From this, we can presume that the maximal CP asymmetry is achieved when $|Y_3|$ is maximal.

The additional condition (E14) yields

$$\frac{Y_1}{m_1} + \frac{Y_2}{m_2} + \frac{Y_3}{m_3} = 0, \quad (\text{E17})$$

$$\frac{\tilde{m}_1}{m_1} X_1 + \frac{\tilde{m}_1}{m_2} X_2 + \frac{\tilde{m}_1}{m_3} X_3 = 1. \quad (\text{E18})$$

Since $m_3 > m_2 > m_1$, we can set $X_2 = X_3 = Y_2 = 0$ for maximal $|Y_3|$. Then, it follows that

$$Y_1 = -\frac{m_1}{m_3} Y_3, \quad X_1 = \frac{m_1}{\tilde{m}_1}. \quad (\text{E19})$$

The second equation in (E13) gives

$$\sqrt{X_1^2 + Y_1^2} + |Y_3| = 1. \quad (\text{E20})$$

The conditions (E19) and (E20) determine $|Y_3|$ as a function of m_1 , m_3 , and \tilde{m}_1 :

$$\begin{aligned} \left(1 - \frac{m_1^2}{m_3^2}\right) |Y_3|^2 - 2|Y_3| + 1 - \frac{m_1^2}{\tilde{m}_1^2} &= 0 \\ \Rightarrow |Y_3| &= 1 - \frac{m_1}{m_3} \sqrt{1 + \frac{m_3^2 - m_1^2}{\tilde{m}_1^2}}, \end{aligned} \quad (\text{E21})$$

where $|Y_3| < 1$ is taken into account. Substituting $Y_2 = 0$ and equation (E21) into equation (E15) yields

$$|\varepsilon_1|^{\max} = \frac{3}{16\pi} \frac{M_1 m_3}{v^2} \left[1 - \frac{m_1}{m_3} \left(1 + \frac{m_3^2 - m_1^2}{\tilde{m}_1^2} \right)^{1/2} \right], \quad (\text{E22})$$

where $m_3^2 - m_1^2 < m_3^2$ is used. This gives the upper bound for $|\varepsilon_1|$.

Appendix F: Formulas for Feynman diagrams

1. Formulas for γ matrices

a. Definition and properties of γ matrices

The γ matrices consist of four $n \times n$ matrices γ^μ (where $\mu = 0, 1, 2, 3$) and satisfy the following anticommutation relations:

$$\{\gamma^\mu, \gamma^\nu\} = \gamma^\mu \gamma^\nu + \gamma^\nu \gamma^\mu = 2\eta^{\mu\nu} \mathbf{1}_{n \times n}. \quad (\text{F1})$$

Equation (F1) is called the Clifford algebra.

b. Definition and properties of chirality γ_5

We define *chirality* γ_5 as

$$\gamma_5 \equiv i\gamma^0 \gamma^1 \gamma^2 \gamma^3. \quad (\text{F2})$$

γ_5 satisfies

$$(\gamma_5)^2 = \mathbf{1}, \quad (\gamma_5)^\dagger = \gamma_5, \quad \gamma_5 \gamma^\mu = -\gamma^\mu \gamma_5, \quad (\text{F3})$$

for $\mu = 0, 1, 2, 3$.

The eigenspaces of γ_5 with eigenvalues ± 1 are referred to as left-chiral and right-chiral, respectively. Let P_L and P_R denote the projection operators onto the left-chiral and right-chiral eigenspaces, respectively. These satisfy

$$P_R = \frac{\mathbf{1} + \gamma_5}{2}, \quad P_L = \frac{\mathbf{1} - \gamma_5}{2}, \quad (\text{F4})$$

and decompose the Dirac spinor ψ into

$$\psi_R = P_R \psi, \quad \psi_L = P_L \psi. \quad (\text{F5})$$

These projection operators satisfy

$$P_R^2 = P_R, \quad P_L^2 = P_L, \quad P_R P_L = P_L P_R = 0. \quad (\text{F6})$$

c. *Feynman slash notation*

The contraction between the 4-vector a^μ and the γ matrix γ^μ is denoted by

$$\not{a} \equiv \gamma^\mu a_\mu = \gamma_\mu a^\mu, \quad (\text{F7})$$

from which it follows that

$$\not{a}^2 = a^2. \quad (\text{F8})$$

d. *Trace formulas*

Traces of gamma matrices are given by

$$\text{tr}(\mathbf{1}) = 4, \quad (\text{F9})$$

$$\text{tr}(\not{a}) = \text{tr}(\not{a}\not{b}\not{c}) = \dots = 0, \quad (\text{F10})$$

$$\text{tr}(\not{a}\not{b}) = (a \cdot b) \text{tr}(\mathbf{1}) = 4(a \cdot b), \quad (\text{F11})$$

$$\text{tr}(\not{a}\not{b}\not{c}\not{d}) = 4[(a \cdot b)(c \cdot d) - (a \cdot c)(b \cdot d) + (a \cdot d)(b \cdot c)], \quad (\text{F12})$$

$$\text{tr}(\gamma_5) = 0, \quad (\text{F13})$$

$$\text{tr}(\not{a}\not{b}\gamma_5) = 0, \quad (\text{F14})$$

$$\text{tr}(\not{a}\not{b}\not{c}\not{d}\gamma_5) = -4i\epsilon^{\mu\nu\rho\sigma} a_\mu b_\nu c_\rho d_\sigma. \quad (\text{F15})$$

2. Properties of Dirac fermions

The positive frequency solution $u^s(p)$ of the Dirac equation satisfies

$$(\not{p} - m)u^s(p) = 0, \quad (\text{F16})$$

while the negative frequency solution $v^s(p)$ satisfies

$$(-\not{p} - m)v^s(p) = 0, \quad (\text{F17})$$

where p is the four-momentum, and s denotes the spin eigenvalue. From the normalization condition of the solution $u^s(p)$

$$\bar{u}^s(p)u^{s'}(p) = 2m\delta_{ss'}, \quad (\text{F18})$$

the orthonormality follows

$$\bar{v}^s(p)v^{s'}(p) = -2m\delta_{ss'}, \quad (\text{F19})$$

$$\bar{u}^s(p)v^{s'}(p) = \bar{v}^s(p)u^{s'}(p) = 0, \quad (\text{F20})$$

$$u^{s\dagger}(\mathbf{p})v^{s'}(-\mathbf{p}) = v^{s\dagger}(\mathbf{p})u^{s'}(-\mathbf{p}) = 0, \quad (\text{F21})$$

$$\bar{u}^s(p)\gamma^\mu u^{s'}(p) = \bar{v}^s(p)\gamma^\mu v^{s'}(p) = 2p^\mu\delta_{ss'}. \quad (\text{F22})$$

Also, $u^{s=\pm}(p)$ and $v^{s=\pm}(p)$ form complete two-dimensional solution spaces satisfying $\not{p} = m$ and $-\not{p} = m$, respectively. The projection operators onto these solution spaces are given by $(\pm\not{p} + m)/2m$, which yield

$$\sum_s u^s(p)\bar{u}^s(p) = \not{p} + m, \quad (\text{F23})$$

$$\sum_s v^s(p)\bar{v}^s(p) = \not{p} - m. \quad (\text{F24})$$

The proportionality coefficients are determined by taking into account the normalization conditions given in equations (F18) and (F19).

3. Formulas for Feynman integrals

a. *Feynman parametrization*

Feynman parametrization is given by

$$\frac{1}{ab} = \int_0^1 dx \frac{1}{[ax + b(1-x)]^2}, \quad (\text{F25})$$

$$\begin{aligned} \frac{1}{abc} &= \int_0^1 dx \int_0^1 dy \int_0^1 dz \frac{2\delta(x+y+z-1)}{(ax+by+cz)^3} \\ &= \int_0^1 dx \int_0^{1-x} dy \frac{2}{[ax+by+c(1-x-y)]^3}. \end{aligned} \quad (\text{F26})$$

b. *Momentum integrals with dimensional regularization*

Momentum integrals with dimensional regularization are given by

$$\begin{aligned} \int \frac{d^n k}{(2\pi)^n} \frac{1}{(m^2 + 2k \cdot p - k^2)^\alpha} \\ = \frac{i\Gamma(\alpha - \frac{n}{2})}{(4\pi)^{\frac{n}{2}}\Gamma(\alpha)} \frac{1}{(m^2 + p^2)^{\alpha - \frac{n}{2}}}, \end{aligned} \quad (\text{F27})$$

$$\begin{aligned} \int \frac{d^n k}{(2\pi)^n} \frac{k^\mu}{(m^2 + 2k \cdot p - k^2)^\alpha} \\ = \frac{i\Gamma(\alpha - \frac{n}{2})}{(4\pi)^{\frac{n}{2}}\Gamma(\alpha)} \frac{p^\mu}{(m^2 + p^2)^{\alpha - \frac{n}{2}}}. \end{aligned} \quad (\text{F28})$$

Setting $\varepsilon \equiv (4-n)/2 \ll 1$, the gamma function gives

$$\Gamma(\varepsilon) = \frac{1}{\varepsilon} - \gamma + \frac{1}{2}\left(\gamma^2 + \frac{\pi^2}{6}\right)\varepsilon + \mathcal{O}(\varepsilon^2), \quad (\text{F29})$$

where γ is the Euler-Mascheroni constant.

[1] A. A. Starobinsky, Spectrum of relict gravitational radiation and the early state of the universe, JETP Lett. **30**,

- [2] K. Sato, First-order phase transition of a vacuum and the expansion of the Universe, *Mon. Not. Roy. Astron. Soc.* **195**, 467 (1981).
- [3] D. Kazanas, Dynamics of the Universe and Spontaneous Symmetry Breaking, *Astrophys. J. Lett.* **241**, L59 (1980).
- [4] A. H. Guth, The Inflationary Universe: A Possible Solution to the Horizon and Flatness Problems, *Phys. Rev. D* **23**, 347 (1981).
- [5] A. D. Linde, A New Inflationary Universe Scenario: A Possible Solution of the Horizon, Flatness, Homogeneity, Isotropy and Primordial Monopole Problems, *Phys. Lett. B* **108**, 389 (1982).
- [6] S. Hawking, The development of irregularities in a single bubble inflationary universe, *Physics Letters B* **115**, 295 (1982).
- [7] A. H. Guth and S. Y. Pi, Fluctuations in the New Inflationary Universe, *Phys. Rev. Lett.* **49**, 1110 (1982).
- [8] A. A. Starobinsky, Dynamics of Phase Transition in the New Inflationary Universe Scenario and Generation of Perturbations, *Phys. Lett. B* **117**, 175 (1982).
- [9] J. M. Bardeen, P. J. Steinhardt, and M. S. Turner, Spontaneous creation of almost scale-free density perturbations in an inflationary universe, *Phys. Rev. D* **28**, 679 (1983).
- [10] N. Aghanim *et al.* (Planck), Planck 2018 results. VI. Cosmological parameters, *Astron. Astrophys.* **641**, A6 (2020), [Erratum: *Astron. Astrophys.* 652, C4 (2021)], [arXiv:1807.06209](https://arxiv.org/abs/1807.06209) [astro-ph.CO].
- [11] S. Alam *et al.* (eBOSS), Completed SDSS-IV extended Baryon Oscillation Spectroscopic Survey: Cosmological implications from two decades of spectroscopic surveys at the Apache Point Observatory, *Phys. Rev. D* **103**, 083533 (2021), [arXiv:2007.08991](https://arxiv.org/abs/2007.08991) [astro-ph.CO].
- [12] A. D. Sakharov, Violation of CP Invariance, C asymmetry, and baryon asymmetry of the universe, *Pisma Zh. Eksp. Teor. Fiz.* **5**, 32 (1967).
- [13] L. Kofman, A. D. Linde, and A. A. Starobinsky, Reheating after inflation, *Phys. Rev. Lett.* **73**, 3195 (1994), [arXiv:hep-th/9405187](https://arxiv.org/abs/hep-th/9405187).
- [14] L. Kofman, A. D. Linde, and A. A. Starobinsky, Towards the theory of reheating after inflation, *Phys. Rev. D* **56**, 3258 (1997), [arXiv:hep-ph/9704452](https://arxiv.org/abs/hep-ph/9704452).
- [15] P. B. Greene, L. Kofman, A. D. Linde, and A. A. Starobinsky, Structure of resonance in preheating after inflation, *Phys. Rev. D* **56**, 6175 (1997), [arXiv:hep-ph/9705347](https://arxiv.org/abs/hep-ph/9705347).
- [16] J. McDonald, Thermally generated gauge singlet scalars as selfinteracting dark matter, *Phys. Rev. Lett.* **88**, 091304 (2002), [arXiv:hep-ph/0106249](https://arxiv.org/abs/hep-ph/0106249).
- [17] L. J. Hall, K. Jedamzik, J. March-Russell, and S. M. West, Freeze-In Production of FIMP Dark Matter, *JHEP* **03**, 080, [arXiv:0911.1120](https://arxiv.org/abs/0911.1120) [hep-ph].
- [18] M. Fukugita and T. Yanagida, Baryogenesis Without Grand Unification, *Phys. Lett. B* **174**, 45 (1986).
- [19] P. Minkowski, $\mu \rightarrow e\gamma$ at a Rate of One Out of 10^9 Muon Decays?, *Phys. Lett. B* **67**, 421 (1977).
- [20] T. Yanagida, Horizontal gauge symmetry and masses of neutrinos, *Conf. Proc. C* **7902131**, 95 (1979).
- [21] M. Gell-Mann, P. Ramond, and R. Slansky, Complex Spinors and Unified Theories, *Conf. Proc. C* **790927**, 315 (1979), [arXiv:1306.4669](https://arxiv.org/abs/1306.4669) [hep-th].
- [22] R. N. Mohapatra and G. Senjanovic, Neutrino Mass and Spontaneous Parity Nonconservation, *Phys. Rev. Lett.* **44**, 912 (1980).
- [23] I. Esteban, M. C. Gonzalez-Garcia, M. Maltoni, T. Schwetz, and A. Zhou, The fate of hints: updated global analysis of three-flavor neutrino oscillations, *JHEP* **09**, 178, [arXiv:2007.14792](https://arxiv.org/abs/2007.14792) [hep-ph].
- [24] M. J. Dolinski, A. W. P. Poon, and W. Rodejohann, Neutrinoless Double-Beta Decay: Status and Prospects, *Ann. Rev. Nucl. Part. Sci.* **69**, 219 (2019), [arXiv:1902.04097](https://arxiv.org/abs/1902.04097) [nucl-ex].
- [25] J. Aasi *et al.* (LIGO Scientific), Advanced LIGO, *Class. Quant. Grav.* **32**, 074001 (2015), [arXiv:1411.4547](https://arxiv.org/abs/1411.4547) [gr-qc].
- [26] F. Acernese *et al.* (VIRGO), Advanced Virgo: a second-generation interferometric gravitational wave detector, *Class. Quant. Grav.* **32**, 024001 (2015), [arXiv:1408.3978](https://arxiv.org/abs/1408.3978) [gr-qc].
- [27] T. Akutsu *et al.* (KAGRA), Overview of KAGRA: Detector design and construction history, *PTEP* **2021**, 05A101 (2021), [arXiv:2005.05574](https://arxiv.org/abs/2005.05574) [physics.ins-det].
- [28] P. Amaro-Seoane *et al.* (LISA), Laser Interferometer Space Antenna, (2017), [arXiv:1702.00786](https://arxiv.org/abs/1702.00786) [astro-ph.IM].
- [29] M. Punturo *et al.*, The Einstein Telescope: A third-generation gravitational wave observatory, *Class. Quant. Grav.* **27**, 194002 (2010).
- [30] B. P. Abbott *et al.* (LIGO Scientific), Exploring the Sensitivity of Next Generation Gravitational Wave Detectors, *Class. Quant. Grav.* **34**, 044001 (2017), [arXiv:1607.08697](https://arxiv.org/abs/1607.08697) [astro-ph.IM].
- [31] K. N. Ananda, C. Clarkson, and D. Wands, The Cosmological gravitational wave background from primordial density perturbations, *Phys. Rev. D* **75**, 123518 (2007), [arXiv:gr-qc/0612013](https://arxiv.org/abs/gr-qc/0612013).
- [32] D. Baumann, P. J. Steinhardt, K. Takahashi, and K. Ichiki, Gravitational Wave Spectrum Induced by Primordial Scalar Perturbations, *Phys. Rev. D* **76**, 084019 (2007), [arXiv:hep-th/0703290](https://arxiv.org/abs/hep-th/0703290).
- [33] B. J. Carr and S. W. Hawking, Black holes in the early Universe, *Mon. Not. Roy. Astron. Soc.* **168**, 399 (1974).
- [34] S. Hawking, Gravitationally collapsed objects of very low mass, *Mon. Not. Roy. Astron. Soc.* **152**, 75 (1971).
- [35] Y. B. Zel'dovich and I. D. Novikov, The Hypothesis of Cores Retarded during Expansion and the Hot Cosmological Model, *Sov. Astron.* **10**, 602 (1967).
- [36] A. Kartavtsev and D. Besak, Baryogenesis via Leptogenesis in an inhomogeneous Universe, *Phys. Rev. D* **78**, 083001 (2008), [arXiv:0803.2729](https://arxiv.org/abs/0803.2729) [hep-ph].
- [37] W. Buchmuller, P. Di Bari, and M. Plumacher, Leptogenesis for pedestrians, *Annals Phys.* **315**, 305 (2005), [arXiv:hep-ph/0401240](https://arxiv.org/abs/hep-ph/0401240).
- [38] G. F. Giudice, M. Peloso, A. Riotto, and I. Tkachev, Production of massive fermions at preheating and leptogenesis, *JHEP* **08**, 014, [arXiv:hep-ph/9905242](https://arxiv.org/abs/hep-ph/9905242).
- [39] N. S. Manton, Topology in the Weinberg-Salam Theory, *Phys. Rev. D* **28**, 2019 (1983).
- [40] F. R. Klinkhamer and N. S. Manton, A saddle-point solution in the weinberg-salam theory, *Phys. Rev. D* **30**, 2212 (1984).
- [41] S. Y. Khlebnikov and M. E. Shaposhnikov, The Statistical Theory of Anomalous Fermion Number Nonconservation, *Nucl. Phys. B* **308**, 885 (1988).
- [42] J. A. Harvey and M. S. Turner, Cosmological baryon and lepton number in the presence of electroweak fermion number violation, *Phys. Rev. D* **42**, 3344 (1990).
- [43] H. Kodama and M. Sasaki, Cosmological Perturbation Theory, *Prog. Theor. Phys. Suppl.* **78**, 1 (1984).

- [44] D. Baumann, *Cosmology* (Cambridge University Press, 2022).
- [45] L. Senatore, S. Tassev, and M. Zaldarriaga, Cosmological Perturbations at Second Order and Recombination Perturbed, *JCAP* **08**, 031, [arXiv:0812.3652 \[astro-ph\]](#).
- [46] W. Buchmuller, P. Di Bari, and M. Plumacher, The Neutrino mass window for baryogenesis, *Nucl. Phys. B* **665**, 445 (2003), [arXiv:hep-ph/0302092](#).
- [47] R. L. Workman *et al.* (Particle Data Group), Review of Particle Physics, *PTEP* **2022**, 083C01 (2022).
- [48] S. Ajimura *et al.* (CANDLES), Low background measurement in CANDLES-III for studying the neutrino-less double beta decay of ^{48}Ca , *Phys. Rev. D* **103**, 092008 (2021), [arXiv:2008.09288 \[hep-ex\]](#).
- [49] C. Alduino *et al.* (CUORE), First Results from CUORE: A Search for Lepton Number Violation via $0\nu\beta\beta$ Decay of ^{130}Te , *Phys. Rev. Lett.* **120**, 132501 (2018), [arXiv:1710.07988 \[nucl-ex\]](#).
- [50] G. Anton *et al.* (EXO-200), Search for Neutrinoless Double- β Decay with the Complete EXO-200 Dataset, *Phys. Rev. Lett.* **123**, 161802 (2019), [arXiv:1906.02723 \[hep-ex\]](#).
- [51] S. Abe *et al.* (KamLAND-Zen), Search for the Majorana Nature of Neutrinos in the Inverted Mass Ordering Region with KamLAND-Zen, *Phys. Rev. Lett.* **130**, 051801 (2023), [arXiv:2203.02139 \[hep-ex\]](#).
- [52] N. Abgrall *et al.* (LEGEND), The Large Enriched Germanium Experiment for Neutrinoless Double Beta Decay (LEGEND), *AIP Conf. Proc.* **1894**, 020027 (2017), [arXiv:1709.01980 \[physics.ins-det\]](#).
- [53] R. Arnold *et al.* (NEMO-3), Results of the search for neutrinoless double- β decay in ^{100}Mo with the NEMO-3 experiment, *Phys. Rev. D* **92**, 072011 (2015), [arXiv:1506.05825 \[hep-ex\]](#).
- [54] R. Arnold *et al.* (NEMO-3), Measurement of the $2\nu\beta\beta$ decay half-life of ^{150}Nd and a search for $0\nu\beta\beta$ decay processes with the full exposure from the NEMO-3 detector, *Phys. Rev. D* **94**, 072003 (2016), [arXiv:1606.08494 \[hep-ex\]](#).
- [55] U.-L. Pen and N. Turok, Shocks in the Early Universe, *Phys. Rev. Lett.* **117**, 131301 (2016), [arXiv:1510.02985 \[astro-ph.CO\]](#).
- [56] C. Cercignani and G. M. Kremer, *The Relativistic Boltzmann Equation: Theory and Applications* (Birkhauser, 2002).
- [57] A. Denner, H. Eck, O. Hahn, and J. Kublbeck, Compact feynman rules for majorana fermions, *Physics Letters B* **291**, 278 (1992).
- [58] A. Denner, H. Eck, O. Hahn, and J. Kublbeck, Feynman rules for fermion-number-violating interactions, *Nuclear Physics B* **387**, 467 (1992).
- [59] W. Buchmuller, P. Di Bari, and M. Plumacher, Cosmic microwave background, matter - antimatter asymmetry and neutrino masses, *Nucl. Phys. B* **643**, 367 (2002), [Erratum: *Nucl.Phys.B* 793, 362 (2008)], [arXiv:hep-ph/0205349](#).